A complex of BRCA2 and PP2A-B56 is required for DNA repair by homologous recombination

Sara Marie Ambjoern[1,2], Julien P. Duxin[1], Emil PT Hertz[1], Isha Nasa[3], Joana Duro[1], Thomas Kruse[1], Blanca Lopez Mendez[1], Beata Rymarczyk[4], Lauren E. Cressey[3], Thomas van Overeem Hansen[5], Arminja Kettenbach[3], Vibe H. Oestergaard[2*], Michael Lisby[2,6*], Jakob Nilsson[1*]

[1] The Novo Nordisk Foundation Center for Protein Research, Faculty of Health and Medical Sciences, University of Copenhagen, Denmark.

[2] Department of Biology, University of Copenhagen, 2200 Copenhagen N, Denmark.

[3] Biochemistry and Cell Biology, Geisel School of Medicine at Dartmouth College, Dartmouth, United States of America.

[4] Department of Biology, University of Konstanz, 78457 Konstanz, Germany.

[5] Department of Clinical Genetics, Copenhagen University Hospital, Rigshospitalet, 2100 Copenhagen, Denmark.

[6] Center for Chromosome Stability, Department of Cellular and Molecular Medicine, University of Copenhagen, DK-2200 Copenhagen N, Denmark.

[*]Correspondence to

Jakob Nilsson: jakob.nilsson@cpr.ku.dk

Michael Lisby: mlisby@bio.ku.dk

Vibe H. Oestergaard: vibe@bio.ku.dk

Abstract

Mutations in the tumour suppressor gene BRCA2 are associated with predisposition to breast and ovarian cancers. BRCA2 has a central role in maintaining genome integrity by facilitating the repair of toxic DNA double-strand breaks (DSBs) by homologous recombination (HR). BRCA2 acts by promoting RAD51 nucleoprotein filament formation on resected single-stranded DNA, but how BRCA2 activity is regulated during HR is not fully understood. Here, we delineate a pathway where ATM and ATR kinases phosphorylate a highly conserved region in BRCA2 in response to DSBs. These phosphorylations stimulate the binding of the protein phosphatase PP2A-B56 to BRCA2 through a conserved binding motif. We show that the phosphorylation-dependent formation of the BRCA2-PP2A-B56 complex is required for efficient RAD51 loading to sites of DNA damage and HR-mediated DNA repair. Moreover, we find that several cancer-associated mutations in BRCA2 deregulate the BRCA2-PP2A-B56 interaction and sensitize cells to PARP inhibition. Collectively, our work uncovers PP2A-B56 as a positive regulator of BRCA2 function in HR with clinical implications for BRCA2 and PP2A-B56 mutated cancers.

Main text

Homologous recombination (HR) is an essential cellular process that repairs severe DNA lesions such as DNA double-strand breaks (DSBs) to ensure genome integrity[1]. Women inheriting monoallelic deleterious mutations in the central HR components BRCA1 and BRCA2 are highly predisposed to breast and ovarian cancers[2,3]. HR-mediated repair takes place during S and G2 phases of the cell cycle and uses a homologous DNA sequence, most often the sister chromatid, as a template to repair DSBs in a high-fidelity manner[1].

BRCA2 plays a central role in HR by facilitating the formation of RAD51 nucleoprotein filaments on resected RPA-coated single-stranded DNA ends, which can then search for and invade a homologous repair template[4–6]. BRCA2 binds monomeric RAD51 through eight central BRC repeats[7–9] and binds and stabilizes RAD51 filaments through a C-terminal domain[10,11]. An N-terminal PALB2 interaction domain recruits BRCA2 to sites of DNA damage as part of the BRCA1-PALB2-BRCA2 complex[12].

HR is a highly regulated process yet many aspects of this regulation are not fully understood[13]. Phosphorylation of BRCA2 and other HR components by DNA damage kinases (ATM/ATR) and cyclin-dependent kinases has been shown to play a role[1,13–15]. In contrast, a direct role of protein phosphatases in HR is less clear in part due to a lack of understanding of how protein phosphatases recognize their substrates[16–18]. Recent discoveries of consensus binding motifs for protein phosphatases[19–21] now allows for precise dissection of their roles in DNA repair processes.

BRCA2 binds PP2A-B56 through a conserved LxxIxE motif and recruits it to DSBs

We previously identified a putative binding site for the serine/threonine protein phosphatase PP2A-B56 in BRCA2, which is of unknown significance[20]. PP2A-B56 is a trimeric complex consisting of a scaffolding subunit (PPP2R1A-B), a catalytic subunit (PPP2CA-B), and a regulatory subunit of the B56 family (isoforms α, β, γ, δ, and ε). PP2A-B56 achieves specificity by binding to LxxIxE motifs in substrates or substrate-specifiers through a conserved binding

pocket present in all isoforms of B56[20,22] (Fig. 1A-B). The LxxIxE motif in BRCA2 is embedded in a hitherto uncharacterized region between BRC repeat 1 and 2 spanning residues 1102-1132, which is highly conserved spanning more than 450 million years of evolution (190 full length vertebrate BRCA2 protein sequences analyzed by Clustal Omega multiple sequence alignment) (Fig.1B and Table S1).To further explore this binding site, we first validated the interaction in human cells, focusing on the main nuclear isoform of B56, B56γ[23]. In HeLa cells, Myc-tagged fragments of BRCA2 spanning BRC repeat 1 and 2 (Myc-BRCA2$^{1001-1255}$) co-purified with Venus-B56γ (Fig. 1C), and reciprocally, all components of the trimeric PP2A-B56 complex co-purified with Venus-BRCA2$^{1001-1255}$ (Fig. S1A, Table S2). Additionally, BRCA2 co-purified with both B56α and B56γ in *Xenopus* egg extracts (Fig. 1D), consistent with an evolutionarily conserved interaction. Mutation of two of the central residues of the LxxIxE motif, L1114 and I1117, to alanines (referred to as the 2A mutant, Fig. 1B) abrogated the interaction to Venus-B56γ (Fig. 1C), showing that the interaction depends on the LxxIxE motif. The direct and LxxIxE motif-dependent interaction between BRCA2 and B56 was confirmed *in vitro* by isothermal titration calorimetry (ITC) (Fig. 1E, Fig. S1B) and gel filtration chromatography (Fig S1C). The K_D is low micromolar, which might explain why the interaction has not been reported previously. Consistent with our binding data, we detected BRCA2 and the BRCA1-PALB2-BRCA2 complex partner BRCA1 in proximity to B56γ in camptothecin (CPT) treated HeLa cells using a biotin proximity labelling approach with TurboID[24]-tagged B56γ coupled to mass spectrometry (Fig. S1D, Table S2).

To determine if BRCA2 could recruit PP2A-B56 to DSBs, we exploited the *Xenopus* egg extract system that allows direct monitoring of proteins binding to DSBs. Either closed circular or linearized DSB-containing plasmids were added to *Xenopus* egg extracts, and proteins co-purifying with the DNA were analyzed by Western blotting following plasmid pulldown. We found that B56γ was enriched on DSB-containing plasmid DNA, and that immuno-depletion of BRCA2 from the extracts diminished the recruitment of B56γ to the same

damaged plasmid (Fig. 1F). Taken together, our results show that BRCA2 binds PP2A-B56 through a highly conserved LxxIxE motif and recruits it to DSBs.

PP2A-B56 binding is required for BRCA2 function in DNA repair by HR

We next asked whether the interaction between BRCA2 and PP2A-B56 is required for the function of BRCA2 in DNA repair. To address this, we constructed an RNAi knockdown and complementation set-up in HeLa DR-GFP Flp-In cells[25] and U2OS Flp-In T-REx cells. This setup allowed transient depletion of endogenous BRCA2 using siRNA-mediated knockdown and complementation with stably expressed siRNA-resistant cDNA constructs of mCherry- or Venus-MBP-tagged full-length BRCA2 WT or 2A (referred to as BRCA2 WT and 2A). Efficient depletion of endogenous BRCA2 and similar expression levels and chromatin association of the complementation constructs were confirmed by immunoblotting (Fig. S2A-C). We then utilized the DR-GFP reporter assay[26] (Fig. 2A, left) to assess HR-mediated DSB repair. Strikingly, complementation with BRCA2 WT but not 2A suppressed the loss of HR-mediated repair resulting from BRCA2 depletion (Fig. 2A, right), suggesting that PP2A-B56 binding is required for the function of BRCA2 in HR. Consistent with this result, we found that expression of a genetically encoded inhibitor of PP2A-B56 binding to LxxIxE motifs similarly diminished HR-mediated repair in the DR-GFP reporter assay[26,27] (Fig. S2D).

BRCA2 is considered essential in most contexts at least in part due to its function in HR and its deletion or depletion leads to lethality[28–32]. To assess the importance of the BRCA2-B56 interaction for cell viability, we performed colony formation assays and determined plating efficiencies for BRCA2 WT and 2A complemented U2OS cells (Fig. 2B). Consistent with the results for HR-mediated repair, expression of BRCA2 WT but not 2A suppressed the diminished viability resulting from BRCA2 depletion (Fig. 2B).

Due to impaired DNA repair, loss of BRCA2 function causes hypersensitivity to various DNA damaging agents including DNA interstrand crosslinking (ICL) agents[33], topoisomerase I inhibitors[34], and Poly-(ADP-ribose) polymerase (PARP) inhibitors[35,36], which is exploited therapeutically[37]. Accordingly, BRCA2 depletion resulted in hypersensitivity to Mitomycin C

(MMC), CPT, and Olaparib (Fig. 2C-E). Consistent with a role for the BRCA2-PP2A-B56 complex in DNA repair, BRCA2 2A expressing cells were significantly more sensitive to these DNA damaging agents than BRCA2 WT expressing cells (Fig. 2C-E).

To investigate the mechanistic basis for the impaired DNA repair in BRCA2 mutant cells, we looked at MMC-induced nuclear RAD51 repair foci in S-phase by immunofluorescence microscopy. BRCA2 depletion abolished the ability to form RAD51 foci (Fig. 2F, Fig. S2E), consistent with the central role of BRCA2 in loading RAD51 to sites of DNA damage[33,38]. Expression of BRCA2 WT but to a lesser extent 2A rescued loss of RAD51 foci resulting from BRCA2 depletion (Fig. 2F). The impairment in RAD51 focus formation observed in the 2A expressing cell line did not arise from significant changes in BRCA2-RAD51 interaction, as similar amounts of RAD51 co-purified with BRCA2 WT and 2A in immunoprecipitation assays (Fig. 2G).

Similar results were obtained when we deleted the entire conserved region, which contains the LxxIxE motif (BRCA2 Δ1100-1131). This also caused a significant decrease in cell viability, DNA damage tolerance, and RAD51 foci formation (Fig. S3A-E), in line with the results of the 2A mutation. We conclude that the interaction to PP2A-B56 is central to the function of BRCA2 in HR-mediated DNA repair.

BRCA2-PP2A-B56 complex formation is stimulated by ATM/ATR-mediated phosphorylation

In several instances, PP2A-B56 interacts with substrate specifiers in a manner regulated by phosphorylation of neighboring sites flanking the LxxIxE motif to allow cross-talk between kinases and phosphatases[20]. The LxxIxE motif of BRCA2 is surrounded by three fully conserved SQ/TQ sites (Fig, 3A, Fig. 1B, Table S1), which are putative consensus phosphorylation sites for the DNA damage response kinases[14]. To validate these phosphorylation sites, we raised phospho-specific antibodies against the first and the last phosphorylation site, S1106 and T1128 (Fig. 3A, Fig. S4A-B for antibody validation). For the pS1106 phosphorylation site, the epitope included phosphorylation of T1104 which is a

putative CDK site. We found that both pT1104/pS1106 and pT1128 phosphorylation are stimulated by CPT-induced DNA damage in S-phase (Fig. 3B). Inhibition of ATM and to a lesser extent ATR kinase reduced the phosphorylation, while inhibition of both fully abrogated it (Fig. 3B, Fig. S4C). To dissect the kinetics of BRCA2 phosphorylation in a more synchronous model system, we turned to *Xenopus* egg extracts, taking advantage of the evolutionary conservation of the region surrounding T1128 (*X. laevis* T1196) (Fig. 3A), which allowed us to use the antibody raised against human BRCA2 pT1128. In this system, addition of a linearized DSB-containing plasmid, but not an intact one, resulted in rapid ATM-dependent T1196 phosphorylation (Fig. S4D-E), which could also be detected on resected linearized DNA (Fig. S4F). Likewise, during the replication-coupled repair of a cisplatin ICL containing plasmid[39], T1196 was also phosphorylated at the time of DSB formation (Fig. 3C). Collectively, these results demonstrate that the SQ/TQ sites in BRCA2 flanking the LxxIxE motif are phosphorylated rapidly by ATM/ATR in response to DSBs.

Next, to directly assess whether phosphorylation of these sites affects the binding to PP2A-B56, we measured the binding affinity between B56 and various phosphorylated BRCA2 peptides by ITC (Fig. 3D, Fig. S5). Phosphorylation of S1123 and S1128 increased the binding affinity four- and two-fold, respectively, while the double phosphorylated peptide (S1123/S1128) had an eight-fold increase in binding affinity (Fig. 3D). In contrast, phosphorylation of S1106 slightly weakened the interaction (Fig. 3D).

To investigate how the phosphorylation status of BRCA2 affects PP2A-B56 binding in cells, we constructed mutants of BRCA2 with all SQ/TQ sites mutated to AQ or DQ (referred to as BRCA2 3AQ and 3DQ), constituting unphosphorylated and phosphorylation-mimetic versions of the protein, respectively (Fig. 3A). We observed that Myc-BRCA2$^{1001\text{-}1255}$ 3AQ co-purified less with Venus-B56γ than Myc-BRCA2$^{1001\text{-}1255}$ WT, whereas Myc-BRCA2$^{1001\text{-}1255}$ 3DQ co-purified more with Venus-B56γ in immunoprecipitation assays (Fig. 3E), consistent with a two-fold increase in binding affinity of a 3DQ peptide measured by ITC (Fig. 3D). Our results argue that collectively these phosphorylations stimulate the binding to PP2A-B56 in cells.

Next, to address whether these phosphorylation sites are important for the function of BRCA2, we investigated the viability, DNA damage tolerance and RAD51 focus formation of cells expressing BRCA2 3AQ and 3DQ in our RNAi and complementation system in U2OS cells (Fig. S2B-C, Fig. 3F-J). Expression of both BRCA2 3AQ and 3DQ resulted in decreased viability and MMC hypersensitivity compared to BRCA2 WT (Fig. 3F-G). Surprisingly, while expression of BRCA2 3AQ led to CPT and Olaparib hypersensitivity and a reduction in RAD51 foci, BRCA2 3DQ was indistinguishable from BRCA2 WT in these assays, suggesting that mimicking phosphorylation is sufficient to sustain some aspects of functionality (Fig. 3H-J). Collectively, these results show that conserved ATM/ATR phosphorylation sites flanking the LxxIxE motif control the interaction to PP2A-B56 and are required for BRCA2 function.

BRCA2 cancer mutations deregulate the interaction to PP2A-B56 and sensitize cells to PARP inhibition.

We next asked whether our findings would be clinically relevant to BRCA2 mutation carriers. Several BRCA2 missense variants of uncertain clinical significance, which are reported in individuals with a hereditary cancer predisposition, localize to the highly conserved B56-interacting region (ClinVar database, NIH). We selected three of them c.3318C>G (S1106R), c.3346A>C (T1116P), and c.3383C>T (T1128I), which localize to the B56-regulating phosphorylation sites or the LxxIxE motif itself (Fig. 4A). Notably, BRCA2 S1106R was recently suggested to be likely benign using a multifactorial likelihood quantitative analysis[40]. We first determined whether these mutations interfere with PP2A-B56 binding. We observed that Myc-BRCA2$^{1001\text{-}1255}$ S1106R and T1116P co-purified more with Venus-B56γ than Myc-BRCA2$^{1001\text{-}1255}$ WT, whereas Myc-BRCA2$^{1001\text{-}1255}$ T1128I co-purified less with Venus-B56γ in immunoprecipitations assays (Fig. 4B). The increased binding of the S1106R mutant was reflected in a two-fold increase in binding affinity as determined by ITC measurements, whereas BRCA2 T1116P and T1128I had K_D values similar to BRCA2 WT (Fig. S6A-B). The stimulatory effect of S1106R likely arise from the generation of a positively charged motif

upstream of the LxxxIxE motif (Fig. 4A) that strengthen binding of PP2A-B56[41]. T1116P generates a putative proline-directed phosphorylation site at position two of the LxxIxE motif (Fig. 4A), which is known to stimulate interaction to PP2A-B56 when phosphorylated[20]. Finally, T1128I likely prevents the stimulatory effect of T1128 phosphorylation.

To address whether these cancer mutations impact on the function of BRCA2, we investigated the cell viability and DNA damage tolerance of cells expressing BRCA2 S1106R, T1116P, and T1128I in our RNAi and complementation system in U2OS cells (Fig. S6C). Expression of BRCA2 S1106R and T1128I resulted in diminished viability compared to expression of BRCA2 WT, and expression of all mutants led to a mild sensitivity to the clinically relevant PARP inhibitor Olaparib (Fig. 4C-D). Collectively, these results suggest that BRCA2 cancer mutations located in the B56-interacting region can deregulate the interaction to PP2A-B56 and sensitize cells to PARP inhibition.

Here, we provide to our knowledge the first example of a protein phosphatase regulating HR by directly binding to an HR component through a specific substrate recognition motif. We propose a model (Fig. 4E) in which ATM/ATR-mediated phosphorylation of BRCA2 in response to DSBs stimulates the recruitment of PP2A-B56 to BRCA2 at the site of the lesion via a conserved LxxIxE motif. The complex of BRCA2 and PP2A-B56 is required for efficient RAD51 loading and HR-mediated repair. This mechanism elegantly enables crosstalk between the DNA damage response and BRCA2-PP2A-B56 complex formation, possibly to ensure proper spatiotemporal formation of the complex.

A major question arising from our findings is what the functional substrate(s) of BRCA2-bound PP2A-B56 are at the site of the DNA lesion. Our results clearly illustrate that PP2A-B56 does not act as a mere off switch for DNA damage response signaling once repair is completed. Rather, the observation that the PP2A-B56 non-binding mutant is deficient in RAD51 focus formation and HR-mediated DSB repair demonstrates that PP2A-B56 plays an active role during HR. BRCA2-bound PP2A-B56 may act to dephosphorylate protein

227 substrates to positively moderate their functions in HR. It is also possible that BRCA2-bound
228 PP2A-B56 is required for dynamic phosphorylation/dephosphorylation cycles of protein
229 substrates at the site of the DNA lesion to drive repair. We anticipate that PP2A-B56 have
230 multiple substrates controlling RAD51 nucleoprotein filament formation and possibly also
231 substrates controlling BRCA2 functions in other processes such as fork protection and cohesin
232 dynamics[42–44]. Interestingly, during mitosis, PP2A-B56 appears to regulate BRCA2 function
233 through an alternative recruitment mechanism[45], suggesting that PP2A-B56 might be a
234 general regulator of BRCA2 functionality throughout the cell cycle.

235 Importantly, our discovery raises the possibility that mutations in PP2A-B56
236 components, which are common in human cancers[46], result in HR deficiencies that may be
237 targeted therapeutically[37]

238

239 **Acknowledgements**

240 Work at the Novo Nordisk Foundation Center for Protein Research is supported by grant
241 NNF14CC0001 and JNI is supported by grants from the Danish Cancer Society (R167-
242 A10951-17-S2), Independent Research Fund Denmark (8021-00101B) and Novo Nordisk
243 Foundation (NNF18OC0053124 and NNF20OC0065098). This work was furthermore
244 supported by the Danish Cancer Society (R146-A9454-16-S2) to S.M.A. and M.L. and the
245 Villum Foundation to V.H.O. and M.L., the Danish National Research Foundation (DNRF115)
246 to M.L., Dansk Kræftforskningsfond to S.M.A., and by the R35GM119455 grant from the
247 National Institute of General Medicine to A.K. We thank the CPR protein production facility
248 for helping to produce and purify recombinant B56 protein and the DanStem Flow Cytometry
249 and Sequencing (FlowCytSeq) platform for technical assistance with flow cytometry. We
250 would also like to thank Helen Piwnica-Worms, Stephen Taylor, and Jeffrey Parvin for the kind
251 gifts of the U2OS Flp-In T-REx, HeLa Flp-In-T-Rex, and HeLa DR-GFP Flp-In cell lines,
252 respectively. Additionally, we thank Tina Thorslund for sharing the pHA-BRCA2 cDNA with us.
253 Furthermore, we want to thank Johannes C. Walter for sharing *Xenopus* antibodies and

reagents as well as Vicenzo Costanzo for sharing the *Xenopus* BRCA2 antibody. The PP2A-B56-LxxIxE motif structure shown in Figure 1A was kindly provided by Rebecca Page.

Author contributions

S.M.A. performed all experimental work with the following exceptions. J.P.D. performed the *Xenopus* egg extract experiments. E.P.T.H., T.K., and V.H.O., contributed to cloning and establishment of RNAi set-up and generated preliminary data. I.N., L.C., and A.K. performed the mass spectrometry experiments. J.D. performed the TurboID experiment and made the model in Figure 4E. B.L.M. generated the ITC data. B.R. generated the *Xenopus* B56 antibodies. T.H. gave clinical input on BRCA2 patient mutations. E.P.T.H. and J.N. purified recombinant proteins, and J.N. performed gel filtration experiments. V.H.O., M.L., and J.N. supervised the project. S.M.A. drafted the manuscript. All authors contributed to the writing of the manuscript.

Conflict of interest statements

JN is on the scientific advisory board for Orion Pharma.

TvOH has received lecture honoraria from Pfizer.

The rest of the authors declare that they have no conflict of interest.

References

1. Chen, C. C., Feng, W., Lim, P. X., Kass, E. M. & Jasin, M. Homology-Directed Repair and the Role of BRCA1, BRCA2, and Related Proteins in Genome Integrity and Cancer. *Annu Rev Cancer Biol* **2**, 313–336 (2018).
2. Antoniou, A. *et al.* Average risks of breast and ovarian cancer associated with BRCA1 or BRCA2 mutations detected in case Series unselected for family history: a combined analysis of 22 studies. *Am J Hum Genet* **72**, 1117–30 (2003).
3. Chen, S. & Parmigiani, G. Meta-analysis of BRCA1 and BRCA2 penetrance. *J Clin Oncol* **25**, 1329–33 (2007).
4. Jensen, R. B., Carreira, A. & Kowalczykowski, S. C. Purified human BRCA2 stimulates RAD51-mediated recombination. *Nature* **467**, 678–83 (2010).
5. Liu, J., Doty, T., Gibson, B. & Heyer, W. D. Human BRCA2 protein promotes RAD51 filament formation on RPA-covered single-stranded DNA. *Nat Struct Mol Biol* **17**, 1260–2 (2010).
6. Thorslund, T. *et al.* The breast cancer tumor suppressor BRCA2 promotes the specific targeting of RAD51 to single-stranded DNA. *Nat Struct Mol Biol* **17**, 1263–5 (2010).
7. Wong, A. K., Pero, R., Ormonde, P. A., Tavtigian, S. V. & Bartel, P. L. RAD51 interacts with the evolutionarily conserved BRC motifs in the human breast cancer susceptibility gene brca2. *J Biol Chem* **272**, 31941–4 (1997).
8. Pellegrini, L. *et al.* Insights into DNA recombination from the structure of a RAD51–BRCA2 complex. *Nature* **420**, 287–293 (2002).
9. Chen, C. F., Chen, P. L., Zhong, Q., Sharp, Z. D. & Lee, W. H. Expression of BRC repeats in breast cancer cells disrupts the BRCA2-Rad51 complex and leads to radiation hypersensitivity and loss of G(2)/M checkpoint control. *J Biol Chem* **274**, 32931–5 (1999).

297 10. Esashi, F., Galkin, V. E., Yu, X., Egelman, E. H. & West, S. C. Stabilization of RAD51
298 nucleoprotein filaments by the C-terminal region of BRCA2. *Nat Struct Mol Biol* **14**, 468–
299 74 (2007).
300 11. Davies, O. R. & Pellegrini, L. Interaction with the BRCA2 C terminus protects RAD51–
301 DNA filaments from disassembly by BRC repeats. *Nat. Struct. Amp Mol. Biol.* **14**, 475
302 (2007).
303 12. Xia, B. *et al.* Control of BRCA2 cellular and clinical functions by a nuclear partner,
304 PALB2. *Mol Cell* **22**, 719–29 (2006).
305 13. Heyer, W.-D., Ehmsen, K. T. & Liu, J. Regulation of Homologous Recombination in
306 Eukaryotes. *Annu. Rev. Genet.* **44**, 113–139 (2010).
307 14. Blackford, A. N. & Jackson, S. P. ATM, ATR, and DNA-PK: The Trinity at the Heart of
308 the DNA Damage Response. *Mol Cell* **66**, 801–817 (2017).
309 15. Esashi, F. *et al.* CDK-dependent phosphorylation of BRCA2 as a regulatory mechanism
310 for recombinational repair. *Nature* **434**, 598–604 (2005).
311 16. Lee, D.-H. *et al.* A PP4 phosphatase complex dephosphorylates RPA2 to facilitate DNA
312 repair via homologous recombination. *Nat. Struct. Mol. Biol.* **17**, 365–372 (2010).
313 17. Kalev, P. *et al.* Loss of PPP2R2A inhibits homologous recombination DNA repair and
314 predicts tumor sensitivity to PARP inhibition. *Cancer Res* **72**, 6414–24 (2012).
315 18. Isono, M. *et al.* BRCA1 Directs the Repair Pathway to Homologous Recombination by
316 Promoting 53BP1 Dephosphorylation. *Cell Rep.* **18**, 520–532 (2017).
317 19. Roy, J. & Cyert, M. S. Cracking the phosphatase code: docking interactions determine
318 substrate specificity. *Sci Signal* **2**, re9 (2009).
319 20. Hertz, E. P. T. *et al.* A Conserved Motif Provides Binding Specificity to the PP2A-B56
320 Phosphatase. *Mol Cell* **63**, 686–695 (2016).
321 21. Ueki, Y. *et al.* A Consensus Binding Motif for the PP4 Protein Phosphatase. *Mol. Cell* **76**,
322 953-964.e6 (2019).
323 22. Wang, X., Bajaj, R., Bollen, M., Peti, W. & Page, R. Expanding the PP2A Interactome by
324 Defining a B56-Specific SLiM. *Structure* **24**, 2174–2181 (2016).

23. McCright, B., Rivers, A. M., Audlin, S. & Virshup, D. M. The B56 Family of Protein Phosphatase 2A (PP2A) Regulatory Subunits Encodes Differentiation-induced Phosphoproteins That Target PP2A to Both Nucleus and Cytoplasm. *J. Biol. Chem.* **271**, 22081–22089 (1996).
24. Branon, T. C. *et al.* Efficient proximity labeling in living cells and organisms with TurboID. *Nat. Biotechnol.* **36**, 880–887 (2018).
25. Starita, L. M. *et al.* A Multiplex Homology-Directed DNA Repair Assay Reveals the Impact of More Than 1,000 BRCA1 Missense Substitution Variants on Protein Function. *Am J Hum Genet* **103**, 498–508 (2018).
26. Pierce, A. J., Johnson, R. D., Thompson, L. H. & Jasin, M. XRCC3 promotes homology-directed repair of DNA damage in mammalian cells. *Genes Dev* **13**, 2633–8 (1999).
27. Kruse, T. *et al.* Mechanisms of site-specific dephosphorylation and kinase opposition imposed by PP2A regulatory subunits. *EMBO J.* **39**, e103695 (2020).
28. Feng, W. & Jasin, M. BRCA2 suppresses replication stress-induced mitotic and G1 abnormalities through homologous recombination. *Nat Commun* **8**, 525 (2017).
29. Ray Chaudhuri, A. *et al.* Replication fork stability confers chemoresistance in BRCA-deficient cells. *Nature* **535**, 382–7 (2016).
30. Evers, B. & Jonkers, J. Mouse models of BRCA1 and BRCA2 deficiency: past lessons, current understanding and future prospects. *Oncogene* **25**, 5885–97 (2006).
31. Patel, K. J. *et al.* Involvement of Brca2 in DNA repair. *Mol Cell* **1**, 347–57 (1998).
32. Kuznetsov, S. G., Liu, P. & Sharan, S. K. Mouse embryonic stem cell–based functional assay to evaluate mutations in BRCA2. *Nat. Med.* **14**, 875 (2008).
33. Yu, V. P. *et al.* Gross chromosomal rearrangements and genetic exchange between nonhomologous chromosomes following BRCA2 inactivation. *Genes Dev* **14**, 1400–6 (2000).
34. Rahden-Staroń, I., Szumiło, M., Grosicka, E., Kraakman van der Zwet, M. & Zdzienicka, M. Z. Defective Brca2 influences topoisomerase I activity in mammalian cells. *Acta Biochim. Pol.* **50**, 139–144 (2003).

353 35. Bryant, H. E. *et al.* Specific killing of BRCA2-deficient tumours with inhibitors of
354 poly(ADP-ribose) polymerase. *Nature* **434**, 913–917 (2005).
355 36. Farmer, H. *et al.* Targeting the DNA repair defect in BRCA mutant cells as a therapeutic
356 strategy. *Nature* **434**, 917–21 (2005).
357 37. Lord, C. J. & Ashworth, A. PARP inhibitors: Synthetic lethality in the clinic. *Science* **355**,
358 1152–1158 (2017).
359 38. Yuan, S. S. *et al.* BRCA2 is required for ionizing radiation-induced assembly of Rad51
360 complex in vivo. *Cancer Res* **59**, 3547–51 (1999).
361 39. Räschle, M. *et al.* Mechanism of Replication-Coupled DNA Interstrand Crosslink Repair.
362 *Cell* **134**, 969–980 (2008).
363 40. Parsons, M. T. *et al.* Large scale multifactorial likelihood quantitative analysis of BRCA1
364 and BRCA2 variants: An ENIGMA resource to support clinical variant classification.
365 *Hum. Mutat.* **40**, 1557–1578 (2019).
366 41. Wang, X. *et al.* A dynamic charge-charge interaction modulates PP2A:B56 substrate
367 recruitment. *eLife* **9**, (2020).
368 42. Schlacher, K. *et al.* Double-strand break repair-independent role for BRCA2 in blocking
369 stalled replication fork degradation by MRE11. *Cell* **145**, 529–42 (2011).
370 43. Brough, R. *et al.* APRIN is a cell cycle specific BRCA2-interacting protein required for
371 genome integrity and a predictor of outcome after chemotherapy in breast cancer. *Embo*
372 *J* **31**, 1160–76 (2012).
373 44. Morales, C. *et al.* PDS5 proteins are required for proper cohesin dynamics and
374 participate in replication fork protection. *J. Biol. Chem.* **295**, 146–157 (2020).
375 45. Ehlén, Å. *et al.* Proper chromosome alignment depends on BRCA2 phosphorylation by
376 PLK1. *Nat. Commun.* **11**, 1819 (2020).
377 46. Mazhar, S., Taylor, S. E., Sangodkar, J. & Narla, G. Targeting PP2A in cancer:
378 Combination therapies. *Biochim. Biophys. Acta BBA - Mol. Cell Res.* **1866**, 51–63
379 (2019).

380 47. Kruse, T. *et al.* Direct binding between BubR1 and B56-PP2A phosphatase complexes
381 regulate mitotic progression. *J. Cell Sci.* **126**, 1086–1092 (2013).
382 48. Kruse, T. *et al.* Mechanisms of site-specific dephosphorylation and kinase opposition
383 imposed by PP2A regulatory subunits. *EMBO J.* **39**, e103695 (2020).
384 49. Larsen, N. B. *et al.* Replication-Coupled DNA-Protein Crosslink Repair by SPRTN and
385 the Proteasome in Xenopus Egg Extracts. *Mol. Cell* **73**, 574-588.e7 (2019).
386 50. Long, D. T., Joukov, V., Budzowska, M. & Walter, J. C. BRCA1 promotes unloading of
387 the CMG helicase from a stalled DNA replication fork. *Mol Cell* **56**, 174–85 (2014).
388 51. Kolinjivadi, A. M. *et al.* Smarcal1-Mediated Fork Reversal Triggers Mre11-Dependent
389 Degradation of Nascent DNA in the Absence of Brca2 and Stable Rad51
390 Nucleofilaments. *Mol. Cell* **67**, 867-881.e7 (2017).
391 52. Long, D. T., Raschle, M., Joukov, V. & Walter, J. C. Mechanism of RAD51-dependent
392 DNA interstrand cross-link repair. *Science* **333**, 84–7 (2011).
393 53. Walter, J. & Newport, J. Initiation of eukaryotic DNA replication: origin unwinding and
394 sequential chromatin association of Cdc45, RPA, and DNA polymerase alpha. *Mol. Cell*
395 **5**, 617–627 (2000).
396 54. Fang, F. & Newport, J. W. Distinct roles of cdk2 and cdc2 in RP-A phosphorylation
397 during the cell cycle. *J. Cell Sci.* **106 (Pt 3)**, 983–994 (1993).
398 55. Eng, J. K., Jahan, T. A. & Hoopmann, M. R. Comet: An open-source MS/MS sequence
399 database search tool. *PROTEOMICS* **13**, 22–24 (2013).
400 56. Elias, J. E. & Gygi, S. P. Target-decoy search strategy for increased confidence in large-
401 scale protein identifications by mass spectrometry. *Nat. Methods* **4**, 207–214 (2007).
402 57. Valot, B., Langella, O., Nano, E. & Zivy, M. MassChroQ: A versatile tool for mass
403 spectrometry quantification. *PROTEOMICS* **11**, 3572–3577 (2011).
404 58. Schwanhäusser, B. *et al.* Global quantification of mammalian gene expression control.
405 *Nature* **473**, 337–342 (2011).
406 59. Tyanova, S. *et al.* Proteomic maps of breast cancer subtypes. *Nat. Commun.* **7**, 10259
407 (2016).

408 60. Lebofsky, R., Takahashi, T. & Walter, J. C. DNA replication in nucleus-free Xenopus egg
409 extracts. *Methods Mol. Biol. Clifton NJ* **521**, 229–252 (2009).
410 61. Kumar, S., Stecher, G., Suleski, M. & Hedges, S. B. TimeTree: A Resource for
411 Timelines, Timetrees, and Divergence Times. *Mol. Biol. Evol.* **34**, 1812–1819 (2017).
412

Methods

Cell culture

U2OS cells, HeLa cells, and derived cell lines from these were cultured in Dulbecco's Modified Eagle Medium with GlutaMAX (Life Technologies) supplemented with 10% fetal bovine serum (Gibco) and 10 units/mL of penicillin and 10 µg/mL of streptomycin (Gibco) at 37°C with 5% CO_2. Expression from the CMV-TetO2 promoter in Flp-In T-REx cells was induced by treatment with 10 ng/mL doxycycline (Clontech) for 24 hours. To synchronize cells to S phase, cells were incubated in growth medium with 2.5 mM thymidine (Sigma) for 24 hours unless otherwise indicated. Cells were released from thymidine by washing twice in PBS and adding growth medium. Mitomycin C (MMC, Sigma), camptothecin (CPT, Sigma), Olaparib (AZD2281, Selleckchem), KU55933 (ATM kinase inhibitor, Selleckchem) and AZ20 (ATR kinase inhibitor, Selleckchem) were added at the indicated doses to the growth medium.

Cloning

A vector for stable high-level expression of BRCA2 in human cells, pcDNA5/FRT/hCMV/Venus-MBP-BRCA2, was generated by swapping the tetracycline-regulated CMV-TetO2 promoter in pcDNA5/FRT/TO with the high-level expression hCMV promoter from phCMV1 using MluI and BspTI restriction sites. To further increase the stability of BRCA2, Venus and MBP where inserted using HindIII and KpnI restriction sites. Finally, full-length BRCA2 was PCR amplified from pHA-BRCA2 (generous gift from Tina Thorslund) and inserted using KpnI and NotI restriction sites to generate pcDNA5/FRT/hCMV/Venus-MBP-BRCA2. To facilitate site-directed mutagenesis of full-length BRCA2, two cloning cassettes were generated using the internal NheI restriction site in combination with either KpnI or NotI encompassing BRCA2 CDS nucleotide positions 1-4584 and 4578-10257, respectively. These fragments were used as templates to introduce mutations in the PP2A-B56 binding region and silent mutations to obtain siRNA-resistance, respectively, and then reintroduced into pcDNA5/FRT/hCMV/Venus-MBP-BRCA2. For generation of

pcDNA5/FRT/hCMV/mCherry-MBP-BRCA2, a synthetic cDNA of mCherry-MBP was synthesized (GeneArt) and swapped for Venus and MBP using HindIII and KpnI restriction sites. A vector for inducible expression of BRCA2 fragments in human cells for biochemistry, pcDNA5/FRT/TO/Myc-BRCA2$^{1001\text{-}1255}$, was generated by PCR amplifying BRCA2$^{1001\text{-}1255}$ with Myc tag-encoding overhangs and subsequent subcloning into pcDNA5/FRT/TO using BamHI and NotI restriction sites. Site-directed mutagenesis was performed to introduce mutations in the PP2A-B56 binding region. Similarly, pcDNA5/FRT/TO/3xFLAG-Venus-BRCA2$^{1001\text{-}1255}$ was generated by PCR amplification of BRCA2$^{1001\text{-}1255}$ and subsequent subcloning into pcDNA5/FRT/TO/3xFLAG-Venus using BamHI and NotI restriction sites. pcDNA5/FRT/TO/HA-TurboID-B56γ was generated by cloning B56γ into pcDNA5/FRT/TO/HA-TurboID. Primer sequences are enclosed in Table S4. Additionally, pcDNA5/FRT/TO/Venus-B56γ1[47], pcDNA5/FRT/TO/mCherry-B56 inhibitor, and pcDNA5/FRT/TO/mCherry-Ctrl inhibitor (3A)[48] were used in this study.

Generation of stable Flp-In T-REx cell lines

U2OS Flp-In T-Rex (a kind gift from Helen Piwnica-Worms), HeLa Flp-In-T-Rex (a kind gift from Stephen Taylor), or HeLa DR-GFP Flp-In (a kind gift from Jeffrey Parvin) cells were grown in medium supplemented with 100 μg/mL Zeocin (Invitrogen). To generate stable cell lines in the Flp-In system, cells were co-transfected with pOG44 (Invitrogen) and a pcDNA5/FRT plasmid of interest using the Fugene 6 transfection kit (Promega) or Lipofectamine 2000 (Invitrogen). After transfection, Flp-In T-REx cells were selected in medium supplemented with 200 μg/mL Hygromycin B (Invitrogen). Individual clones were selected and analyzed for expression. For T-REx cells, selection included 5 μg/mL blasticidin S HCl (Sigma).

Transfection

For transient protein expression, cells were transfected with Lipofectamine 2000 (Invitrogen) and the plasmid of interest and incubated for 48 hours unless otherwise stated. For BRCA2

knockdown, cells were transfected twice with 10 nM Silencer Select BRCA2 s2084 siRNA and 10 nM Silencer Select BRCA2 s2085 siRNA (Ambion) using Lipofectamine RNAiMAX (Invitrogen) 24 and 48 hours before the experiment. A luciferase oligo (5'-CGUACGCGGAAUACUUCGAdTdT-3', Sigma) was used for control (Ctrl).

DR-GFP reporter assay

To analyze HR efficiency for full-length BRCA2 constructs, HeLa DR-GFP Flp-In cells parental or stably expressing siRNA resistant mCherry-MBP-BRCA2 were transfected with Ctrl or BRCA2 siRNA as described above. The second siRNA transfection was combined with transient transfection with or without an I-SceI-encoding plasmid. After 48 hours, cells were trypsinized, dissolved in 2% BSA in PBS, stained with 1 μg/mL DAPI, and analyzed on a BD LSRFortessa flow cytometer (BD biosciences) for FSC (A, W, H), SSC (A), DAPI (A), and GFP (A). Debris and doublets were excluded by gating. Living cells were gated by excluding DAPI positive cells. The fraction of GFP positive cells was quantified and the background (without I-SceI endonuclease) was subtracted for each condition. Graphs were constructed in PRISM. For the B56 inhibitor experiment, HeLa DR-GFP Flp-In cells were transiently transfected with a plasmid encoding an mCherry-tagged version of the B56 substrate inhibitor or a control version of the inhibitor described previously[48] either with or without an I-SceI-encoding plasmid. After 48 hours, cells were prepared and analyzed as described above but using mCherry (A) to gate transfected cells. The fraction of GFP positive cells in the mCherry positive population was quantified, and the background (without I-SceI endonuclease) was subtracted for each condition. Graphs were constructed in PRISM, and a Student's t-test was performed to determine the p-value.

Colony formation assay

U2OS Flp-In T-REx cells parental or expressing siRNA-resistant venus-MBP-BRCA2 constructs were transfected with Ctrl or BRCA2 siRNA as described above. Then, cells were either treated with 0, 3, or 10 ng/mL Mitomycin C for 24 hours followed by reseeding into

normal growth medium or reseeded directly and either treated for 24 hours with 0, 5, or 15 nM CPT or continuously maintained in medium containing 0, 5.6, 16.7, or 50 nM Olaparib. Reseeding was performed by trypsinizing the cells, dissolving into growth medium, and counting the number of cells using the Scepter Cell Counter (Merck), followed by seeding a known number of cells into 6-well plates containing growth medium. After 11 days, the cells were fixed and stained in 0.5% methylviolet, 25% methanol. The plates were scanned on a GelCount (Oxford Optronix), and the number of colonies were quantified using the GelCount software. The plating efficiency (%) for each well was calculated as the number of colonies divided by the number of cells seeded times 100. The surviving fraction for each dose of drug was calculated by normalizing the plating efficiency to that of the unperturbed condition. Graphs were constructed in PRISM (Graphpad), and one-way ANOVA analyses with Dunnett's multiple comparison tests were performed comparing the averages of each condition to the siBRCA2 + WT condition for a minimum of three independent experiments.

Immunofluorescence microscopy

U2OS Flp-In T-REx cells parental or expressing siRNA-resistant venus-MBP-BRCA2 constructs were seeded in µ-Slide 8-well dishes (Ibidi). Alongside Ctrl or BRCA2 siRNA transfection as described above, cells were synchronized to S phase with a single 24-hour 2 mM thymidine block. Cells were released from the block, treated with 3 µM MMC for 1 hour, and then allowed to recover for 8 hours in normal growth medium. Cells were fixed and permeabilized by incubation in 4% formaldehyde for 10 minutes, 0.1% Triton-X-100 in PBS-T for 10 minutes, and 25 mM glycine for 20 minutes, followed by blocking in 3% BSA (Sigma) in PBS-T for 30 minutes. Cells were incubated with primary antibody, rabbit-anti-RAD51 (Bioacademia 70-001) 1:1000 in blocking solution, for 90 minutes, followed by washing in TBS-T and incubation with secondary antibody, AlexaFluor 546 nm Goat-anti-rabbit IgG (Life Technologies, A-11010) 1:1000 and 1 µg/mL DAPI, in blocking solution for 45 minutes. Finally, cells were washed in PBS-T and analysed on a Deltavision Elite microscope using a 40X oil

523 objective. Images were deconvoluted using SoftWoRx (GE healthcare), and Z stacks
524 combined using the Quick projection function. The number of RAD51 foci in each nucleus was
525 quantified using the polygon finder function. Graphs were constructed in PRISM.
526
527 **Antibodies**
528 Commercially available antibodies against the following proteins were used for Western
529 blotting in the indicated dilutions: BRCA2 (OP95, Calbiochem, 1:1000), RAD51 (70-001,
530 Bioacademia, 1:1000), mCherry (RFP) (PM005, MBL International, 1:1000), Myc (Sc-40,
531 Santa Cruz, 1:750), PALB2 (A301-246A – M, Bethyl, 1:1000), GAPDH (Sc-25778, Santa Cruz,
532 1:5000), tubulin (Ab6160, Abcam, 1:5000), histone 3 (Ab1791, Abcam, 1:1000), pS345-CHK1
533 (#2341, Cell signaling, 1:1000), pS1981-ATM (MAB3806, Millipore, 1:2000), PP2A-C (05-421,
534 Sigma-Aldrich, 1:1000). Additionally, an antibody against GFP was used (Serum produced by
535 Moravian, affinity purified against full-length GFP). Phospho-specific polyclonal antibodies
536 against BRCA2-pT1104/pS1106 and BRCA2-pT1128 were raised in rabbits using
537 phosphorylated peptides of BRCA2 for immunization, affinity purification, and validation
538 (SNHNL(pT)P(pS)QKAEI for BRCA2-pT1104/pS1106 (21st Century Biochemicals) and
539 CQFEF(pT)QFRKPS for BRCA2-pT1128 (Moravian)).
540 Antibodies against *Xenopus* MCM6[49], BRCA2[50], BRCA2[51] (Fig. S4D), RAD51[52],
541 RPA[53], and ORC2[54] were described previously. Additional antibodies against the following
542 *Xenopus* proteins were raised in rabbits against the following peptides: BRCA2 (Ac-
543 KPHIKEDQNEPESNSEYC-amide, New England Peptide) as described previously[51], WRN
544 (H2N-MTSLQRKLPEWMSVKC-amide, New England Peptide), B56α
545 (MSAISAAEKVDGFTRKSVRK, Peptide Speciality Laboratories GmbH), and B56γ
546 (MPNKNKKDKEPPKAGKSGKS, Peptide Speciality Laboratories GmbH). The antibody
547 against *Xenopus* BRCA2-pT1196 was raised against human BRCA2-pT1128 (see above).
548
549 **Whole cell extracts, immunoprecipitation, and Western blotting.**

For whole cell extracts, cells were lysed in ice-cold RIPA buffer (10 mM Tris, pH 7.4, 150 mM NaCl, 1 mM EDTA, 1% NP-40, 0.5% sodium deoxycholate, 0.1% SDS), and cell lysates were cleared by centrifugation at 20000 g at 4°C. Protein concentrations in cell lysates were determined using Bradford protein assay kit (Bio-Rad) or Pierce BCA protein assay kit (Thermo Fisher Scientific).

For GFP-trap immunoprecipitation of Venus and Venus-B56γ, HeLa Flp-In T-Rex cells stably expressing doxycycline-inducible Venus or Venus-B56γ were transiently transfected with the indicated constructs of pcDNA5/FRT/TO/Myc-BRCA2$^{1001\text{-}1255}$, induced with 10 ng/mL doxycycline, and incubated with 3 ng/mL MMC for 24 hours prior to cell harvest. Cells were lysed in ice-cold low salt lysis buffer (50 mM Tris, pH 7.4, 50 mM NaCl, 1 mM EDTA, 0.1% Igepal). Cell lysates were cleared by centrifugation at 20000 g at 4°C, and proteins were purified by GFP-trap (ChromoTek) immunoprecipitation for 1 hour at 4°C. Beads were washed in ice-cold no salt wash buffer (50 mM Tris pH 7.4, 20% glycerol, 1 mg/mL BSA) prior to elution.

For GFP-trap immunoprecipitation of Venus and Venus-BRCA2$^{1001\text{-}1255}$, HeLa cells were transiently transfected with pcDNA5/FRT/TO/Venus or pcDNA5/FRT/TO/Venus-BRCA2$^{1001\text{-}1255}$, synchronized to S phase as described above, released for 2 hours and then treated for 2 hours with 100 nM CPT prior to cell harvest. Cells were lysed and proteins purified by GFP-trap immunoprecipitation in low salt lysis buffer as described above. Beads were washed in low salt lysis buffer prior to elution.

For GFP-trap immunoprecipitation of Venus-MBP-BRCA2, U2OS Flp-In T-REx stably expressing constructs of Venus-MBP-BRCA2 were lysed and proteins immunoprecipitated as described above but in a standard salt lysis buffer (50 mM Tris, pH 7.4, 150 mM NaCl, 1 mM EDTA, 0.1% Igepal).

For immunoprecipitations of endogenous BRCA2, U2OS Flp-In T-REx cells were synchronized to S-phase as described above, released for 1 hour, and treated for 1 hour with 2 μM CPT in presence or absence of 25 μM KU55933 (ATM kinase inhibitor) and 5 μM AZ20 (ATR kinase inhibitor). Cells were lysed in RIPA buffer, and proteins were immunoprecipitated

on BRCA2 antibody-conjugated (OP95, Calbiochem) Rec-protein G Sepharose 4B beads (Invitrogen) for 1 hour at 4°C and washed in RIPA buffer prior to elution.

All buffers were supplemented with 1 mM DTT, Complete protease inhibitor cocktail (Roche), and PhosSTOP phosphatase inhibitor cocktail (Roche). For λ phosphatase treatment experiments, immunoprecipitants on beads were washed in buffer without phosphatase inhibitor and incubated with λ phosphatase (Sigma Aldrich) in the applied buffer for 20 minutes at 30°C before elution. Immunoprecipitants were eluted in 2X NuPage LDS sample buffer (Invitrogen). Whole cell extracts and immunoprecipitations were analyzed by SDS-PAGE and Western blotting or mass spectrometry analysis. For Western blotting, samples were boiled for 5 minutes in NuPage LDS sample buffer and run on NuPage Bis-Tris 4-12% protein gels (Invitrogen), and proteins were transferred to PVDF membranes (Immobilon-FL, Merck). For dot blots, the indicated peptides were spotted onto nitrocellulose membranes (Hybond-C extra, Amersham Biosciences) in 5-fold dilutions (highest amount 2 μg). *Xenopus* samples (see below) were prepared in 2X Laemmli sample buffer, boiled for 5 min, run on 4–12% Criterion XT Bis-Tris Protein Gels (Bio-rad), and proteins were transferred to Polyscreen (R) PVDF transfer membranes (PerkinElmer). All membranes were blocked in 5% skim milk or BSA, incubated in primary antibody solution overnight at 4°C, washed in TBS-T, incubated in secondary antibody for 1 hour, washed again in TBS-T, and imaged with the Odyssey® CLx (LI-COR) or incubated with ECL reagent and imaged on an ImageQuant LAS4000 (Cytiva). Quantification of Western blots were carried out in Image Studio Lite (LI-COR).

Fractionation assay

U2OS Flp-In T-REx cells stably expressing Venus-MBP-BRCA2 were transfected with BRCA2 siRNA as described above prior to lysis in low salt lysis buffer. Upon clearing of the lysates, supernatants were stored as the soluble fractions. The pellets were resuspended and lysed in RIPA buffer supplemented with benzonase nuclease (Merck Millipore). Lysates were

603 centrifuged again, and the supernatants were stored as the chromatin fractions. The soluble
604 and chromatin fractions were analyzed by SDS-PAGE and Western blotting.
605
606 **Biotin proximity labeling assay**
607 HeLa Flp-In T-Rex encoding doxycycline-inducible TurboID-B56γ were induced with 4 ng/mL
608 doxycycline alongside synchronization to S phase as described above. Cells were released
609 for 2 hours in presence of 100 nM CPT, and 50 μM biotin (Sigma) was added 30 minutes
610 before harvest. Biotinylated proteins were purified on High Capacity Streptavidin Agarose
611 beads (Thermo Scientific) in RIPA buffer and proteins were identified by mass spectrometry.
612
613 **Protein expression**
614 BRCA2$^{1089\text{-}1143}$ WT and 2A (L1114A-I1117A) were cloned into pGEX-4T-1 to generate N-
615 terminally GST-tagged fusion proteins. Constructs were transformed into *E. coli* BL21 (DE3)
616 cells and expression was induced by addition of 0.5 mM IPTG at 37°C for 3 h. Bacterial pellets
617 were resuspended in ice-cold lysis buffer (50 mM Tris-HCl pH 7.4, 300 mM NaCl, 10%
618 glycerol, 5 mM β-mercaptoethanol, 1 mM phenylmethyl sulfonyl fluoride, and complete EDTA-
619 free Protease Inhibitor Cocktail tablets (Roche)) and lysed in an EmulsiFlex-C3 High Pressure
620 Homogenizer (Avestin). Lysates were cleared at 26,200g for 30 min at 4°C and supernatants
621 were incubated with pre-washed Glutathione Sepharose 4 Fast Flow beads (GE Healthcare)
622 for 90 min at 4°C with mixing. Beads were washed six times in ice-cold lysis buffer, and GST-
623 fusion proteins were eluted at 22°C for 30 min, 1250 rpm in elution buffer (50 mM Tris pH 8.8,
624 300 mM NaCl, 10% glycerol, 5 mM β-mercaptoethanol, 20 mM reduced glutathione). Eluates
625 were further purified by gel filtration on a Superdex 75 10/300 GL column. His-tagged B56α
626 was expressed in the *E. coli* strain BL21 Rosetta2 (DE3) R3 T1 at 18°C for 20 hours using 0.5
627 mM IPTG. The bacterial pellets were resuspended in ice-cold buffer L (50mM NaP, 300mM
628 NaCl, 10% Glycerol, 0.5 mM TCEP, pH 7.5) containing complete EDTA-free Protease Inhibitor
629 Cocktail tablets and lysed with an EmulsiFlex-C3 High Pressure Homogenizer. The lysate was

centrifuged at 18500 g for 30 minutes and the supernatant filtered through a 0.22 µm PES filter and loaded onto a 1 mL Ni column (GE healthcare) in buffer L with 10 mM immidazole, washed and eluted. The eluate was loaded on a Superdex 200 PG 16/60 equilibrated with SEC buffer (50 mM NaP, 150 mM NaCl, 0.5 mM TCEP, 10% Glycerol, pH 7.50) and fractions analyzed by SDS-PAGE and verified by mass spectrometry.

Isothermal titration calorimetry (ITC)

Peptides were purchased from Peptide 2.0 Inc. (Chantilly, VA, USA). The purity obtained in the synthesis was 95 – 98% as determined by high performance liquid chromatography (HPLC) and subsequent analysis by mass spectrometry. Both recombinant B56α and synthetic BRCA2 peptides were extensively dialyzed prior to ITC experiments against the ITC buffer (50 mM sodium phosphate pH 7.5, 150 mM NaCl, 0.5 mM TCEP). All experiments were performed on a MicroCal Auto-iTC200 (Malvern Panalytical) instrument at 25°C. Both peptide and B56α concentrations were determined using a spectrophotometer by measuring the absorbance at 280 nm and applying values for the extinction coefficients as computed from the corresponding sequences by the ProtParam program (http://web.expasy.org/protparam/). The BRCA2 peptides were loaded into the syringe and titrated into the calorimetric cell containing B56α. The reference cell was filled with distilled water. Control experiments with the peptides injected in the sample cell filled with buffer were carried out under the same experimental conditions. These control experiments showed negligible heats of dilution in all cases. The titration sequence consisted of a single 0.4 µl injection followed by 19 injections, 2 µl each, with 150 s spacing between injections to ensure that the thermal power returns to the baseline before the next injection. The stirring speed was 750 rpm. The heats per injection normalized per mole of injectant *versus* the molar ratio [BRCA2 peptide]/[B56α] were fitted to a single-site model. Data were analysed with MicroCal PEAQ-ITC (version 1.1.0.1262) analysis software (Malvern Panalytical).

Gel filtration

To analyze the binding between BRCA2 and B56α by gel filtration, 100 μg of B56α was incubated with 40 μg of GST or GST-BRCA2$^{1089-1143}$ in buffer G (150 mM NaCl, 25 mM Tris 8.0, 10% glycerol, 1mM DTT) in a total volume of 525 µl. Following incubation, the sample was loaded on a Superdex 200 10/300 column (GE Healthcare) and fractions were analysed by SDS-PAGE and Coomassie blue staining.

Label-free LC-MS/MS analysis

Pull-downs were analyzed on a Q-Exactive Plus quadrupole or Fusion Orbitrap Lumos mass spectrometer (ThermoScientific) equipped with Easy-nLC 1000 or 12000 (ThermoScientific) and nanospray source (ThermoScientific). Peptides were resuspended in 5% methanol / 1% formic acid and analyzed as previously described[48].

Raw data were searched using COMET (release version 2014.01) in high resolution mode[55] against a target-decoy (reversed)[56] version of the human proteome sequence database (UniProt; downloaded 2/2020, 40704 entries of forward and reverse protein sequences) with a precursor mass tolerance of +/- 1 Da and a fragment ion mass tolerance of 0.02 Da, and requiring fully tryptic peptides (K, R; not preceding P) with up to three mis-cleavages. Static modifications included carbamidomethylcysteine and variable modifications included: oxidized methionine. Searches were filtered using orthogonal measures including mass measurement accuracy (+/- 3 ppm), Xcorr for charges from +2 through +4, and dCn targeting a <1% FDR at the peptide level. Quantification of LC-MS/MS spectra was performed using MassChroQ[57] and the iBAQ method[58]. Missing values were imputed from a normal distribution in Perseus to enable statistical analysis[59]. For further analysis, proteins had to be identified in the B56γ +dox +biotin or Venus-BRCA2 samples with more than 1 total peptide and quantified in 2 or more replicates. B56γ or BRCA2 protein abundances were normalized to be equal across all samples. Statistical analysis was carried out in Perseus by two-tailed Student's t-test.

***Xenopus* egg extract work**

Xenopus egg extracts preparation and reactions

Xenopus egg extracts were prepared as described before[60]. For replication of pICL^{Pt}, the plasmid was first licensed in high-speed supernatant (HSS) extract for 30 min at RT at a final DNA concentration of 7.5 ng/mL. DNA replication was then initiated by adding two volumes of nucleoplasmic egg extract (NPE). For all other non-replicating reactions DNA was supplemented to NPE at a final concentration of 15 ng/mL. When indicated ATM inhibitor (KU-55933, Selleckchem), ATR inhibitor (AZ20, Sigma) or DNA-PK inhibitor (NU 7441, Selleckchem) were added to NPE to a final concentration of 100 μM 10 min prior to initiating the reaction. To visualize DNA replication intermediates, reactions were supplemented with [α-^{32}P] dCTP (Perkin Elmer) and 1.5 μL of each time point was added to 5 mL of stop buffer (5% SDS, 80 mM Tris pH 8.0, 0.13% phosphoric acid, 10% Ficoll). Proteins were digested by adding 1 mL of Proteinase K (20 mg/mL) (Roche) for 1 hour at 37°C. Replication intermediates were separated by 0.9% native agarose gel electrophoresis and visualized using a phosphorimager.

DNA constructs

pICL^{Pt} was prepared as previously described[39]. To generate closed circular or linear DNA substrates, pBlueScript was either untreated or linearized with XhoI and the respective species purified via gel electrophoresis.

Immunoprecipitations and immunodepletions

To immunodeplete BRCA2 from NPE, one volume of Protein A Sepharose Fast Flow (PAS) (GE Health Care) beads was bound to five volumes of affinity purified BRCA2 antibody (1 mg/mL) overnight at 4°C. The beads were then washed once with PBS, once with ELB (10 mM HEPES pH 7.7, 50 mM KCl, 2.5 mM $MgCl_2$, and 250 mM sucrose), twice with ELB supplemented with 0.5 M NaCl, and twice with ELB. One volume of NPE was then depleted by mixing with 0.2 volumes of antibody-bound beads incubated at room temperature for 15

min. The supernatant was recovered, and the depletion procedure repeated 3 additional times. The mock depletion was performed similarly using purified IgG from pre-immune serum.

For immunoprecipitation experiments, 5 mL of PAS beads were incubated with 10 mg of the indicated affinity purified antibody. The sepharose beads were washed twice with PBS and three times with IP buffer 1 (10 mM Hepes pH 7.7, 50 mM KCl, 2.5 mM $MgCl_2$, 0.25% NP-40). 5 mL of NPE was diluted with 20 mL of IP buffer and incubated with antibody prebound beads for 1 hour at RT. The beads were then washed three times with IP buffer and resuspended in 50 mL of 2x Laemmli sample buffer before analysis by Western blotting.

Plasmid pull-down

For plasmid pull-down experiments, 10 mL of streptavidin-coupled magnetic beads (Dynabead M-280, Invitrogen) per pull-down reaction were equilibrated with wash buffer 1 (50 mM Tris-HCl, pH 7.5, 150 mM NaCl, 1mM EDTA pH 8, 0.02% Tween 20) and then incubated with 12 pmol of biotinylated LacI at RT for 40 min. The beads were washed four times with pull-down buffer (10 mM Hepes pH 7.7, 50 mM KCl, 2.5 mM $MgCl_2$, 250 mM sucrose, 0.02% Tween 20). 225 ng of either closed circular or linear pBlueScript was bound to beads for 45 min. The beads were then washed twice with pull-down buffer and resuspended in 15 mL of NPE supplemented with Tween 20 to a final concentration of 0.02%. The reaction was incubated for 15 min at RT, washed twice in pull-down buffer and resuspended in 30 mL of 2X Laemmli sample buffer before analysis by Western blotting.

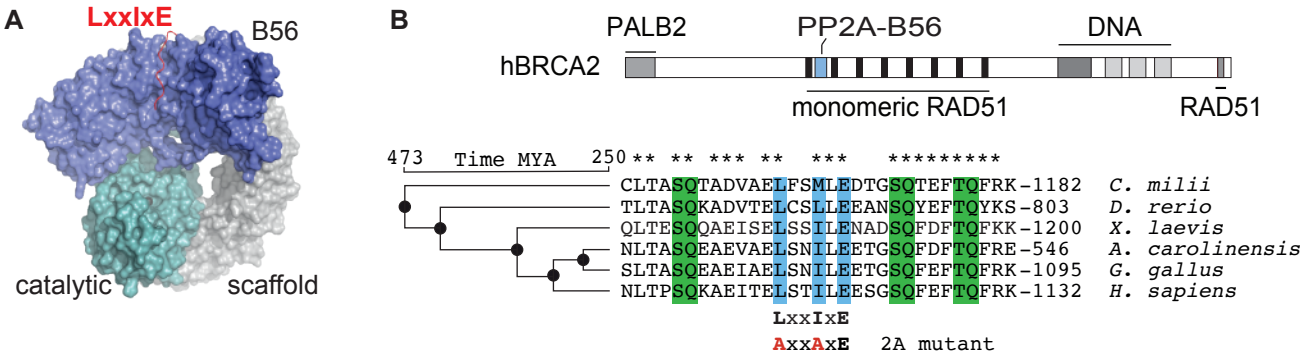

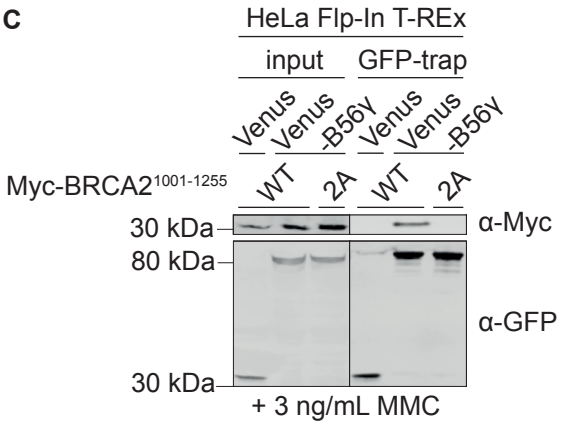

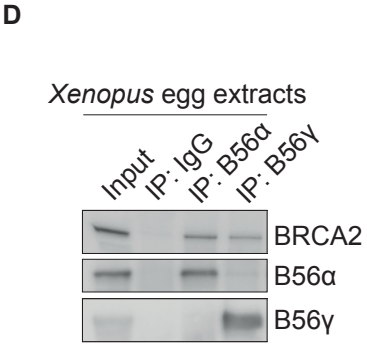

E

Isothermal titration calorimetry

B56α complex	K_D (μM)
BRCA2$^{1108-1126}$ WT	5.2 ± 0.40
BRCA2$^{1108-1126}$ 2A	No binding

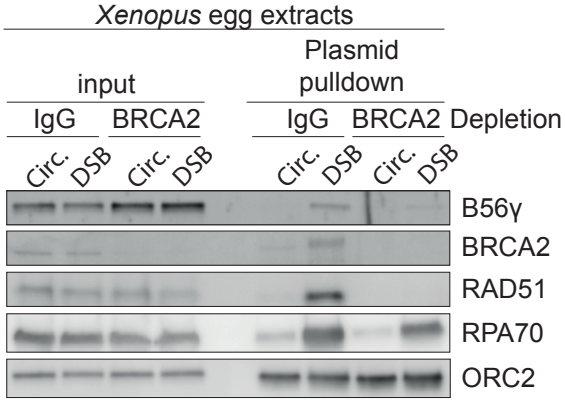

Figure 1.

Figure 1. BRCA2 binds PP2A-B56 through a conserved LxxIxE motif and recruits it to DSBs.

A. Structure of the PP2A-B56 holoenzyme with an LxxIxE motif-containing peptide bound. B. Top: Domain organization of human BRCA2 with selected interaction domains and the PP2A-B56 binding motif indicated. Bottom: Sequence alignment of vertebrate BRCA2 protein sequences. LxxIxE motif is marked in blue and SQ/TQ sites in green. The sequence of the human 2A (L1114A, I1117A) mutation is shown. *, conserved residues. Evolution tree using the TimeTree database[61] (timetree.org) is shown. MYA, million years ago. C. Western blot of the co-immunoprecipitation of Myc-BRCA2$^{1001\text{-}1255}$ WT or 2A with Venus or Venus-B56γ from HeLa Flp-In T-REx cells in presence of 3 ng/mL MMC representative of three independent experiments. D. Western blot of the co-immunoprecipitation of BRCA2 with B56 subunits from *Xenopus* egg extracts representative of two independent experiment. E. Dissociation constants (K_D) for the interaction between the indicated BRCA2 peptides and B56α measured by isothermal titration calorimetry. F. Western blot of a pulldown of an intact or linearized DSB-containing plasmid from mock (IgG) or BRCA2 immunodepleted *Xenopus* egg extracts representative of two independent experiments.

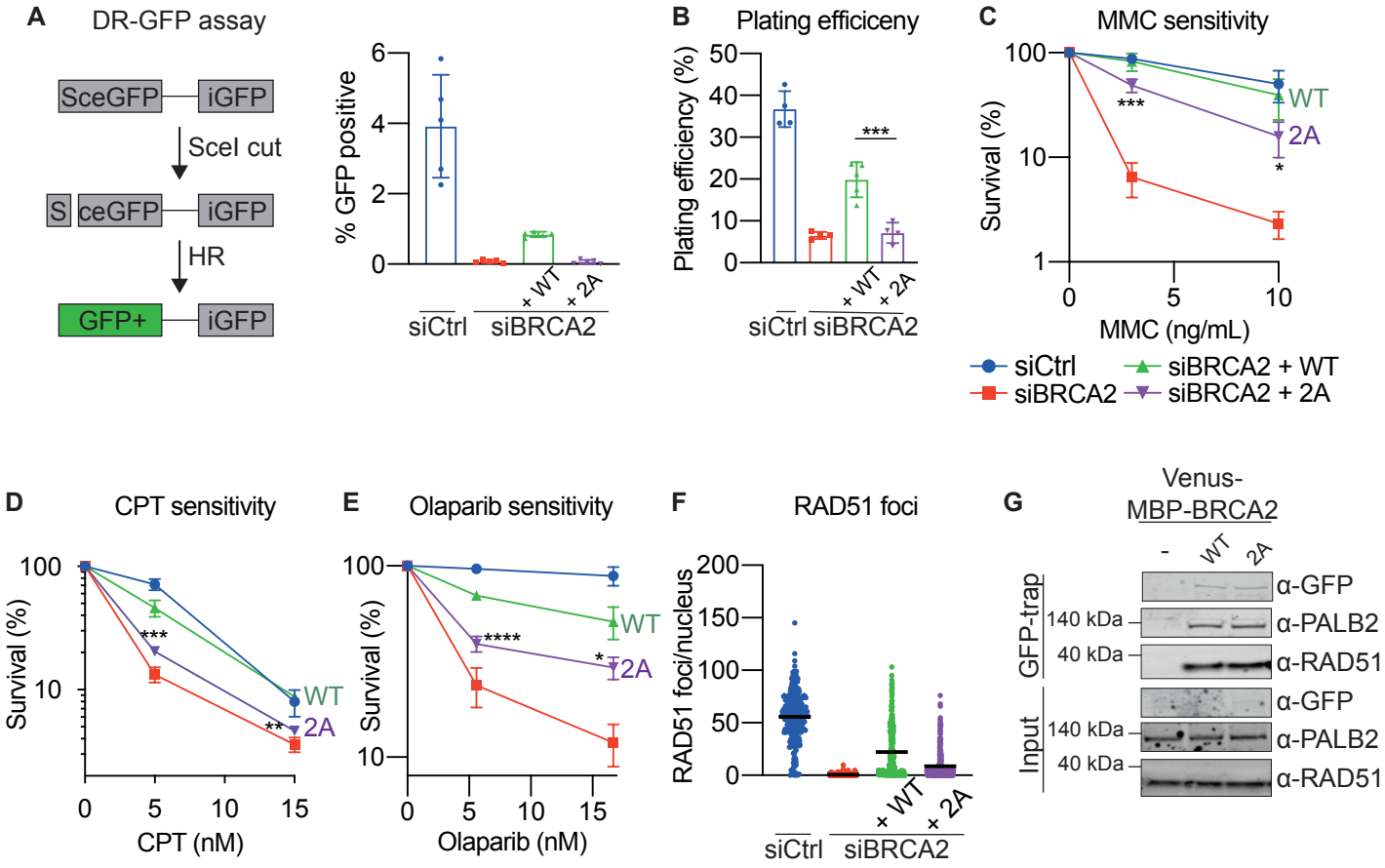

Figure 2.

Figure 2. The BRCA2-PP2A-B56 complex is required for DNA repair by HR.

A. Left: Schematic of the DR-GFP reporter assay. Right: Percentage of GFP positive (HR completed) HeLa DR-GFP Flp-In cells expressing the indicated siRNA resistant mCherry-MBP-BRCA2 cDNAs after transfection with Ctrl or BRCA2 siRNAs and an I-SceI-encoding plasmid, quantified by flow cytometry. Background values (without I-SceI) were subtracted. Error bars represent means and standard deviations. B-F: U2OS Flp-In T-REx cells stably expressing siRNA resistant WT or 2A Venus-MBP-BRCA2 cDNAs were transfected with Ctrl or BRCA2 siRNAs. B-E. Colony formation assays showing plating efficiency (B), MMC sensitivity (C), CPT sensitivity (D), and Olaparib sensitivity (E). Error bars indicate means and standard deviations. One-way ANOVA analyses with Dunnett's multiple comparison tests were performed to compare each condition to siBRCA2 + WT for a minimum of three independent experiments. *=p<0.5, **=p<0.1, ***=p<0.001, ****=p<0.0001. F. RAD51 nuclear foci in cells synchronized to S-phase, treated for 1 hour with MMC, and allowed to recover for 8 hours before immunofluorescence microscopy. Each dot represents an individual nucleus, and means are indicated. The experiment is a representative of three independent experiments. G. Western blot of the co-purification of RAD51 and PALB2 with Venus-MBP-BRCA2 WT and 2A from U2OS Flp-In T-REx cells representative of three independent experiments.

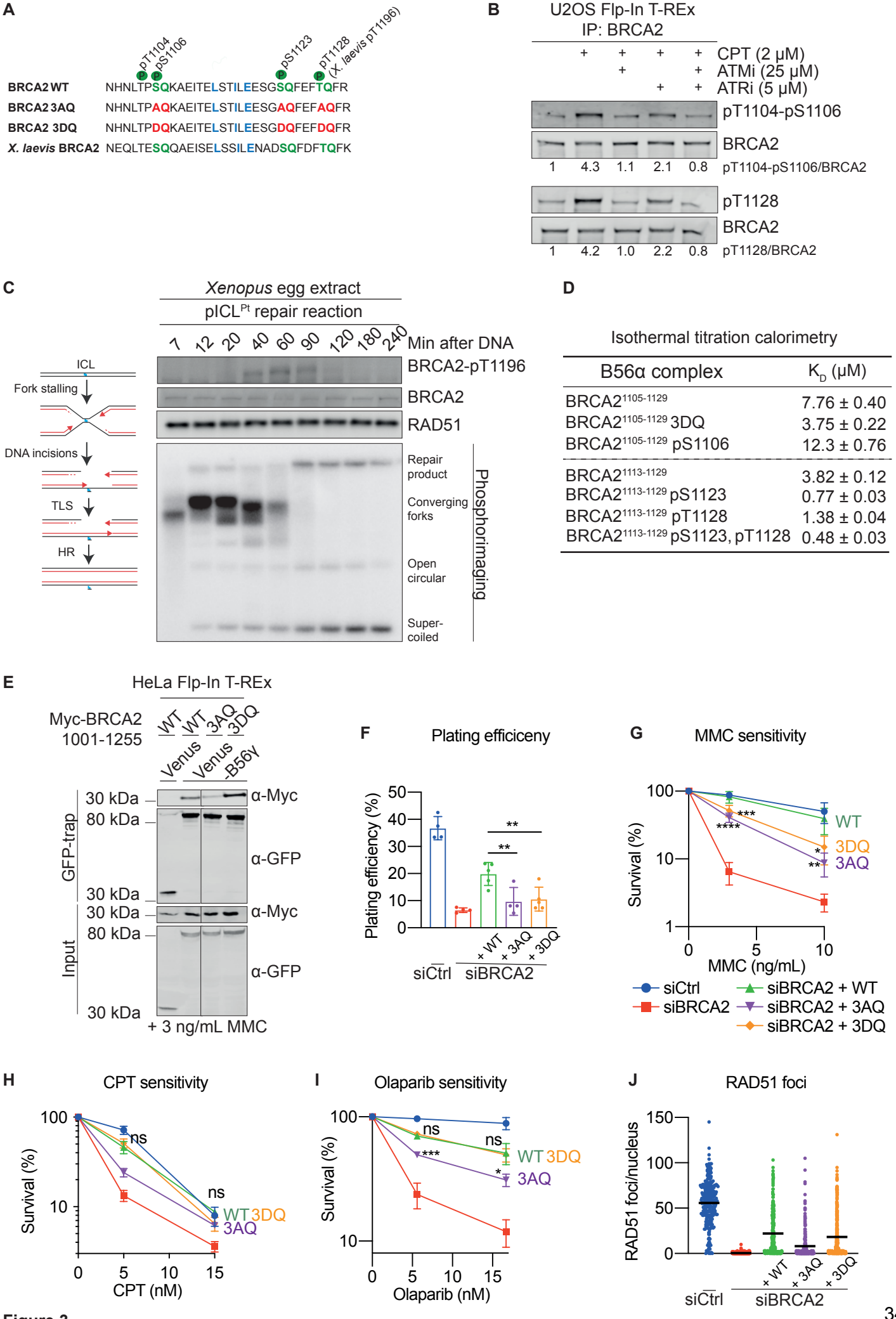

Figure 3

Figure 3. PP2A-B56 binding to BRCA2 is stimulated by ATM/ATR-mediated phosphorylation

A. Schematic of the conserved B56 binding region of human and *Xenopus laevis* BRCA2 with LxxIxE motif, relevant phosphorylation sites, and introduced mutations indicated. B. Western blots of BRCA2 immunoprecipitates from U2OS Flp-In T-Rex cells synchronized to S-phase and treated for 1 hour with 2 μM CPT in presence or absence of ATM and ATR inhibitors representative of two independent experiments. The relative ratio of phosphorylated to total BRCA2 is indicated. C. Left: schematic of an cisplatin ICL repair reaction. Right: A replication-coupled $pICL^{Pt}$ repair reaction in *Xenopus* egg extracts. Top: Western blot analysis. Bottom: Analysis of a reaction run in the presence of [α-^{32}P]dCTP by agarose gel electrophoresis and visualization on a phosphoimager. Representative of two independent experiments. D. Dissociation constants (K_D) for the interactions between the indicated BRCA2 peptides and B56α measured by isothermal titration calorimetry. E. Western blot of co-immunoprecipitated Myc-$BRCA2^{1001\text{-}1255}$ WT, 3AQ, or 3DQ with Venus-B56γ from HeLa Flp-In T-Rex cells in presence of 3 ng/mL MMC representative of three independent experiments. The Myc-$BRCA2^{1001\text{-}1255}$ WT data (lanes 1-2) are identical to Fig. 1C. F-J. U2OS Flp-In T-REx cells stably expressing siRNA resistant WT, 3AQ, or 3DQ Venus-MBP-BRCA2 cDNAs were transfected with Ctrl or BRCA2 siRNA. The siCtrl, siBRCA2, and siBRCA2 + WT data are identical to Fig. 2B-F. F-I. Colony formation assays showing plating efficiency (F), MMC sensitivity (G), CPT sensitivity (H), and Olaparib sensitivity (I) as in Fig. 2B-E for a minimum of three independent experiments except for 3AQ in H which is n=2. Ns, non-significant. J. RAD51 nuclear foci examined as in Fig. 2F.

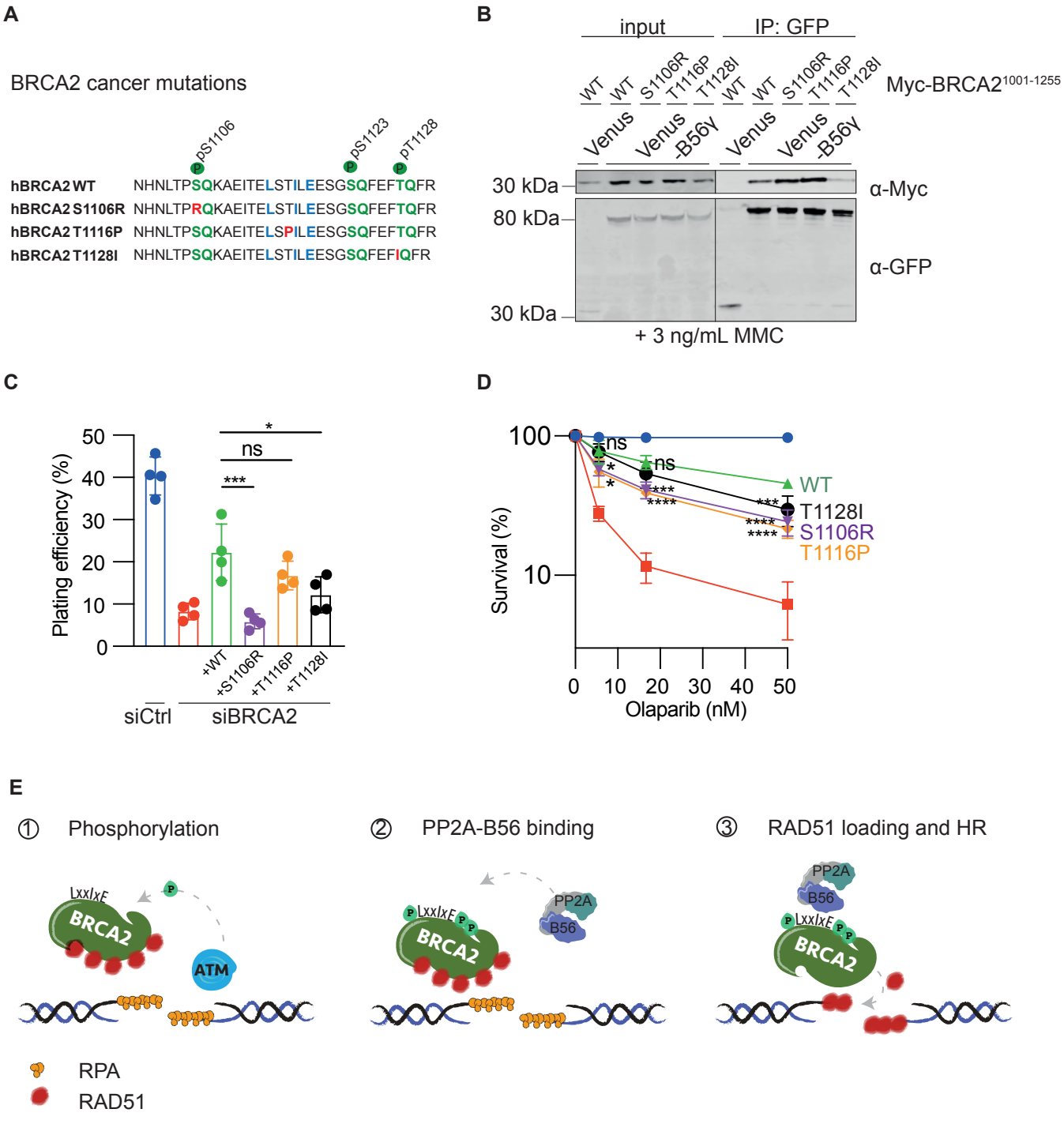

Figure 4.

Figure 4. BRCA2 cancer-associated mutations deregulate PP2A-B56 binding and sensitize cells to PARP inhibition.

A. Schematic of the B56 binding region of human BRCA2 with the introduced cancer-associated mutations indicated. B. Western blot of co-immunoprecipitated Myc-BRCA2$^{1001\text{-}1255}$ WT, S1106R, T1116P, or T1128I with Venus-B56γ from HeLa Flp-In T-Rex cells in presence of 3 ng/mL MMC representative of three independent experiments. C-D. U2OS Flp-In T-REx cells stably expressing siRNA resistant WT, S1106R, T1116P, and T1128I Venus-MBP-BRCA2 cDNAs were transfected with Ctrl or BRCA2 siRNA. Colony formation assays were performed to determine plating efficiency (C), and Olaparib sensitivity (D). Error bars indicate means and standard deviations. One-way ANOVA analyses with Dunnett's multiple comparison tests were performed to compare each condition to siBRCA2 + WT for four independent experiments. *=p<0.5, ***=p<0.001, ****=p<0.0001. Ns, non-significant. E. Model. In the presence of DNA damage such as DSBs, ATM and ATR kinases phosphorylate BRCA2 on S1106, S1123, and T1128. This stimulates the binding of PP2A-B56 through a conserved LxxIxE motif, thus recruiting PP2A-B56 to the broken DNA. The phosphorylation-regulated binding of PP2A-B56 is required for the ability of BRCA2 to load RAD51 onto damaged DNA and repair DSBs via HR.

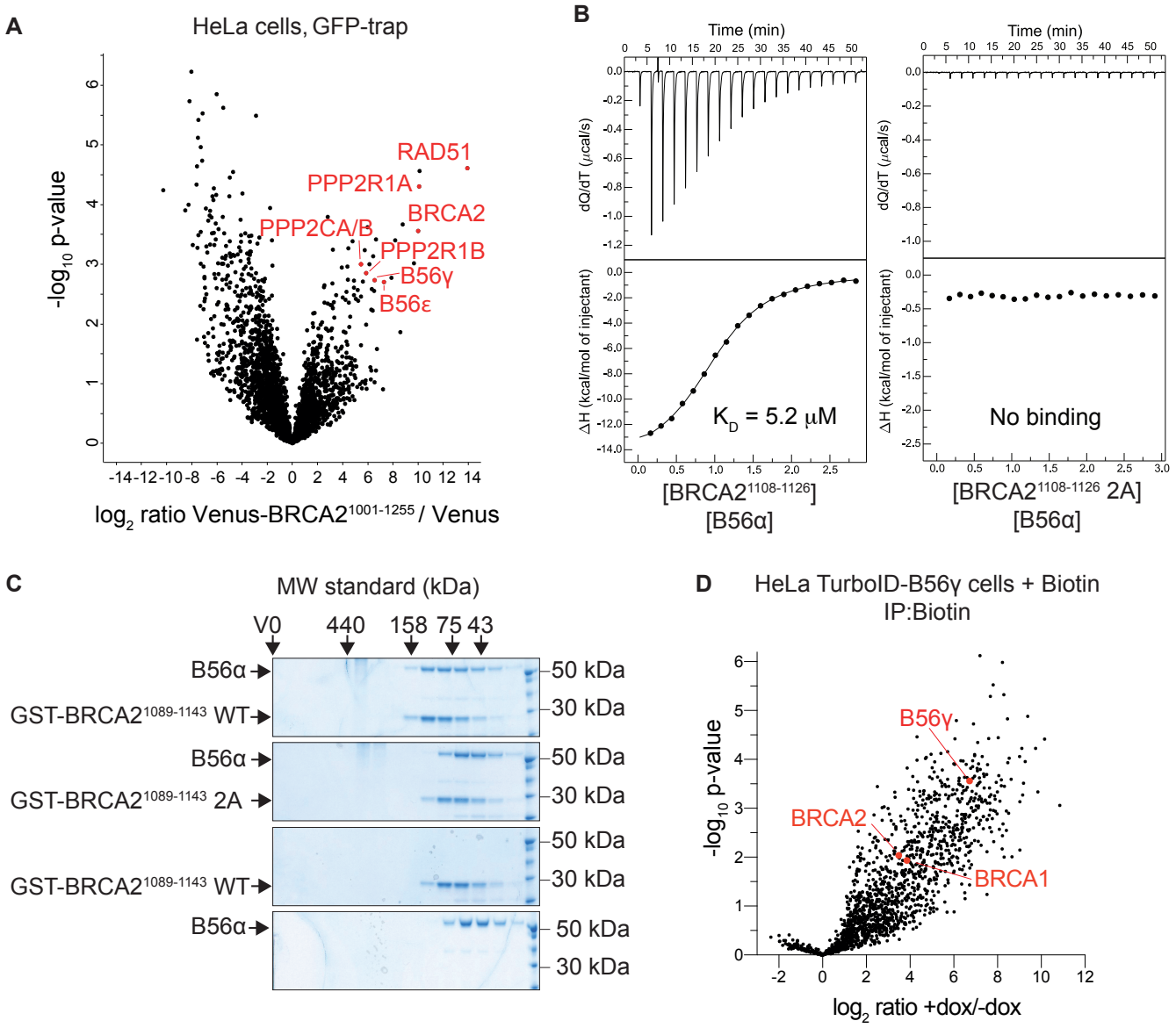

Figure S1.

Figure S1. Data related to Figure 1.

A. Volcano plot of proteins co-purifying with Venus-BRCA2$^{1001-1255}$ versus Venus in HeLa cells in presence of 100 nM CPT identified by mass spectrometry. B. Isothermal titration calorimetry binding curves for the interaction between BRCA2$^{1108-1126}$ WT or 2A peptides and B56α. C. Colloidal stained gel showing the gel filtration chromatography of B56α with GST-BRCA2$^{1089-1143}$ WT or 2A. D. Screen for B56γ proximity partners. Volcano plot of biotinylated proteins from biotin proximity labelling and mass spectrometry analysis from HeLa Flp-In T-REx cells expressing doxycycline (dox)-inducible TurboID-B56γ in presence of 100 nM CPT.

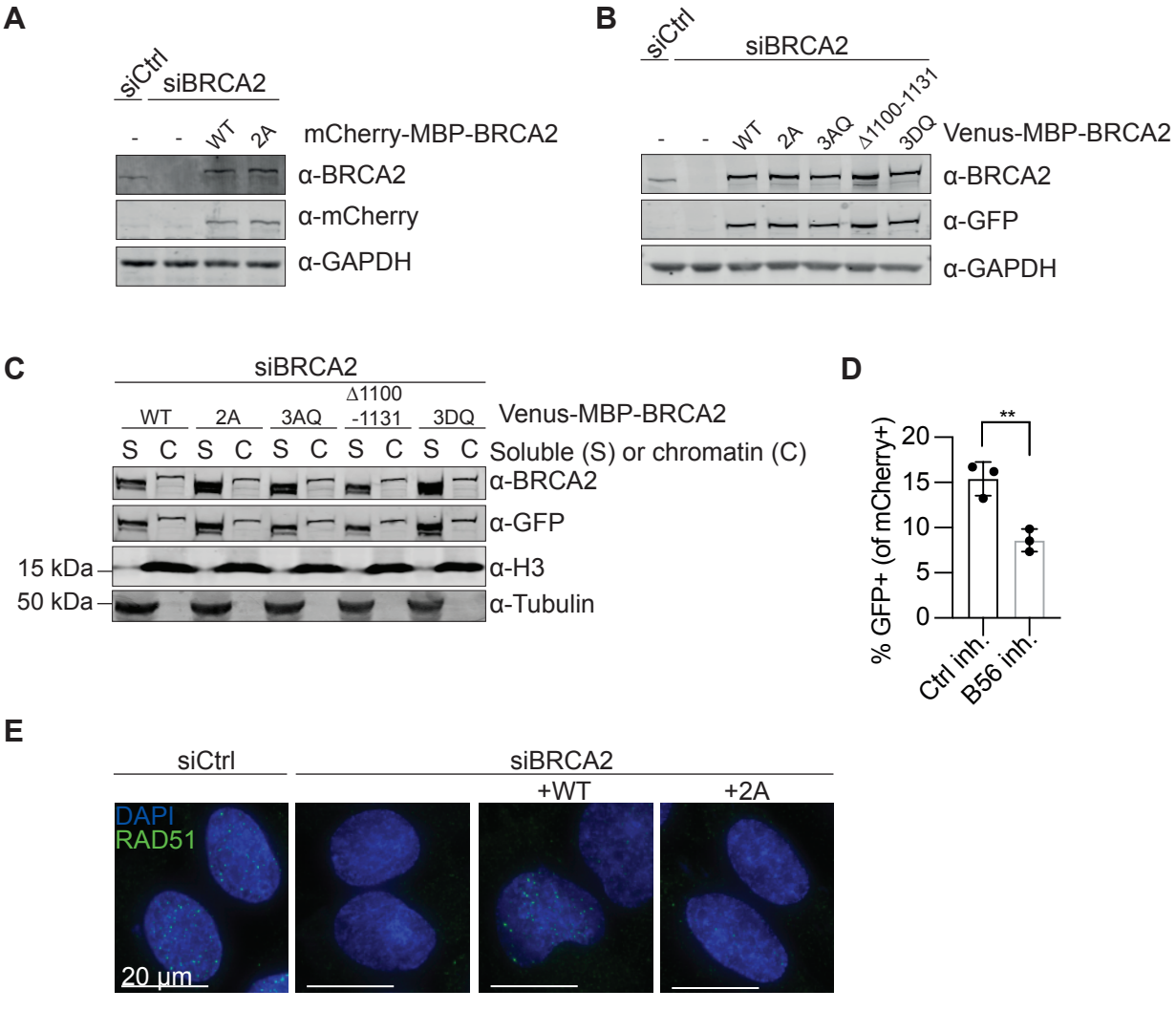

Figure S2

Figure S2. Data related to Figure 2.

A. Western blot of cell extracts from HeLa DR-GFP Flp-In cells stably expressing siRNA resistant mCherry-MBP-BRCA2 WT or 2A cDNA constructs after transfection with Ctrl or BRCA2 siRNA. B. Western blot of cell extracts from U2OS Flp-In T-REx cells stably expressing the indicated siRNA resistant Venus-MBP-BRCA2 constructs after transfection with Ctrl or BRCA2 siRNA. C. Western blot of fractionated chromatin from U2OS Flp-In T-REx cells stably expressing the indicated siRNA resistant Venus-MBP-BRCA2 constructs after BRCA2 siRNA transfection. D. Percentage of GFP positive (HR completed) HeLa DR-GFP Flp-In cells within the mCherry positive population of cells transfected with an SceI-encoding plasmid alongside an mCherry-tagged PP2A-B56 inhibitor or a control inhibitor. Background values (without I-SceI) were subtracted. Error bars represent means and standard deviations. Student's t-test was performed, ** = $p<0.01$. E. Representative immunofluorescence microcopy images of RAD51 foci from Figure 2F.

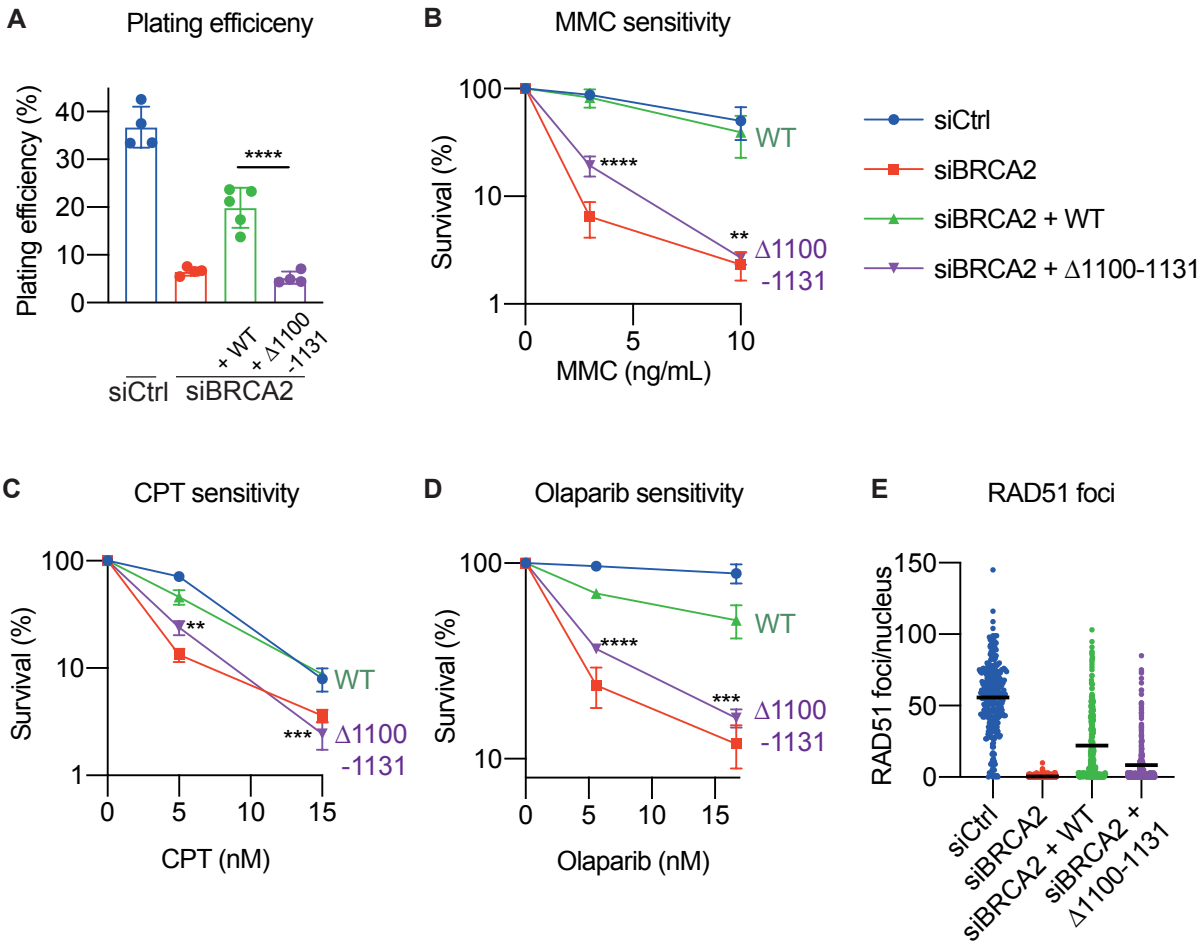

Figure S3.

Figure S3. Data related to Figure 2.

A-E. U2OS Flp-In T-REx cells stably expressing siRNA resistant WT or ∆1100-1131 Venus-MBP-BRCA2 cDNAs were transfected with Ctrl or BRCA2 siRNA. The siCtrl, siBRCA2, and siBRCA2 + WT data is identical to Fig. 2B-F. A-D. Colony formation assays showing plating efficiency (A), MMC sensitivity (B), CPT sensitivity (C), and Olaparib sensitivity (D) as in Fig. 2B-E. E. MMC-induced RAD51 nuclear foci as in Fig. 2F.

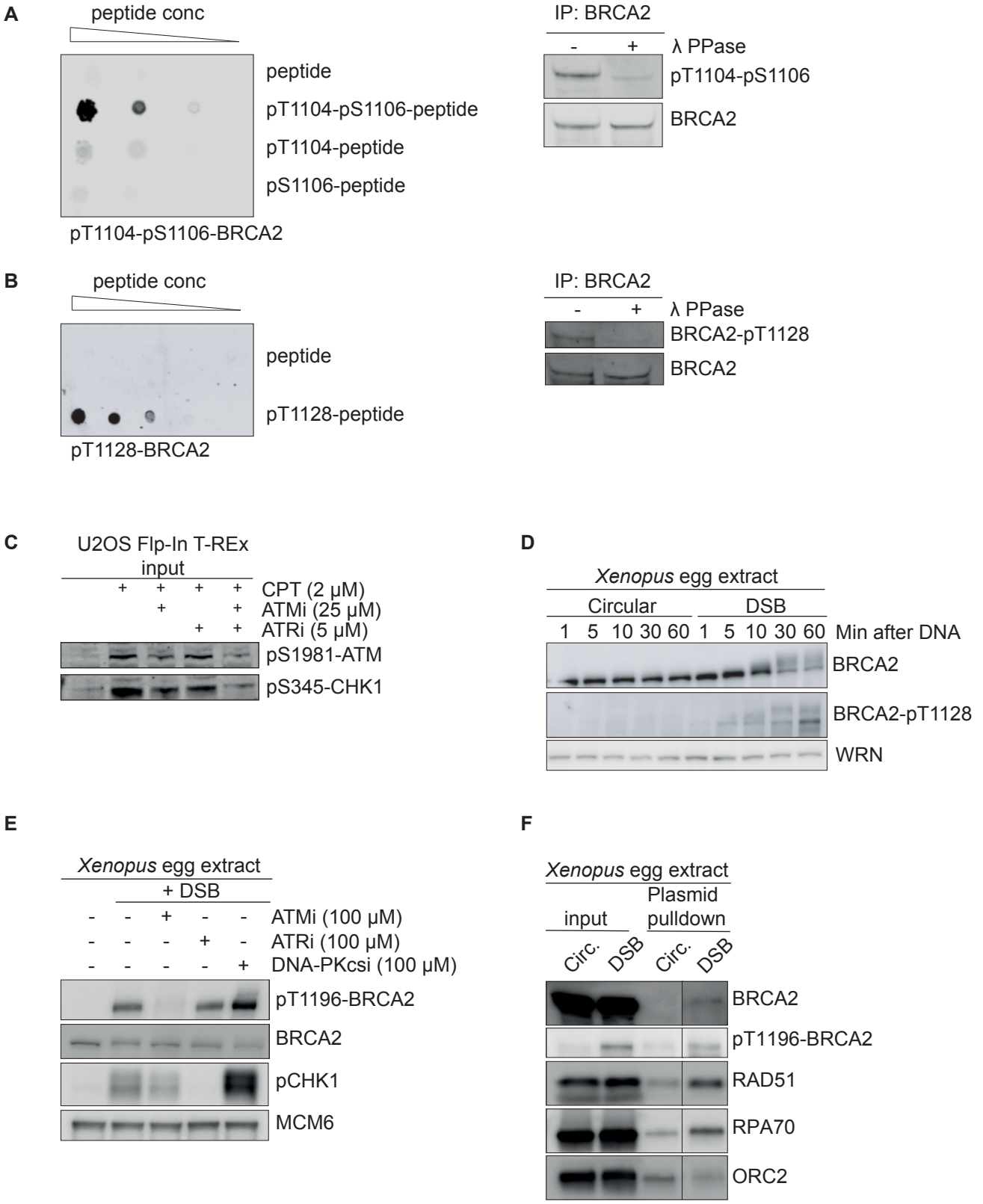

Figure S4.

Figure S4. Data related to Figure 3.

A. Validation of the phospho-specificity of the pT1104/pS1106-BRCA2 polyclonal antibody. Left: dot blot of non-phosphorylated and phosphorylated versions of the BRCA2 peptide SNHNL(p)TP(p)SQKAEI. Right: Western blot of lambda phosphatase treated endogenous immunoprecipitated BRCA2 from U2OS Flp-In T-REx cells synchronized to S phase and treated for 1 hour with 2 μM CPT. B. Validation of the phospho-specificity of the pT1128-BRCA2 polyclonal antibody as in A. using the non-phosphorylated and phosphorylated BRCA2 peptide CQFEF(p)TQFRKPS for dot blotting. C. Western blot of cell extracts from U2OS Flp-In T-REx cells synchronized to S phase and treated for 1 hour with 2 μM CPT in presence or absence of ATM and ATR inhibitors representative of two independent experiments. D. Western blot of BRCA2 in *Xenopus* egg extracts after addition of an intact circular (Circ) or linearized DSB-containing plasmid representative of two independent experiments. E. Western blot of *Xenopus* egg extracts after addition of a linearized DSB-containing plasmid in presence of ATM, ATR, or DNA-PKcs inhibitors representative of two independent experiments. F. Western blot of proteins pulled down with an intact or linearized DSB-containing plasmid from *Xenopus* egg extracts representative of three independent experiments.

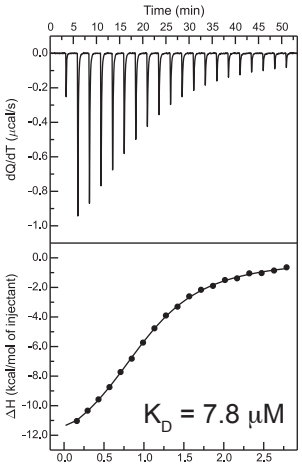

[BRCA2$^{1105\text{-}1129}$]/ [B56α]

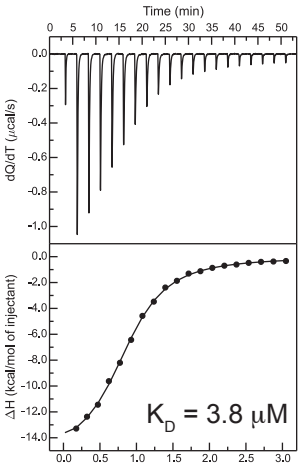

[BRCA2$^{1105\text{-}1129}$ *3DQ*]/ [B56α]

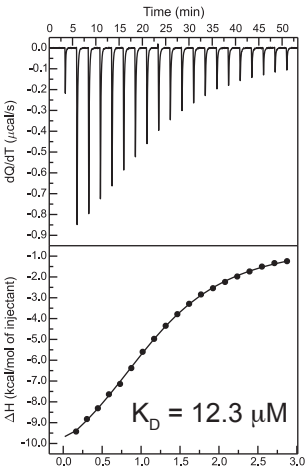

[BRCA2$^{1105\text{-}1129}$ *pS1106*]/ [B56α]

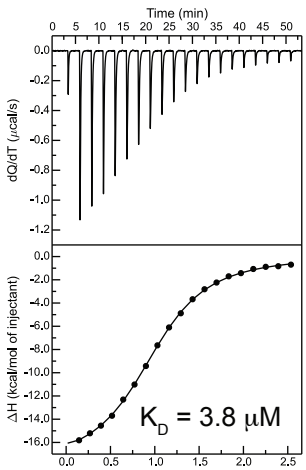

[BRCA2$^{1113\text{-}1129}$]/ [B56α]

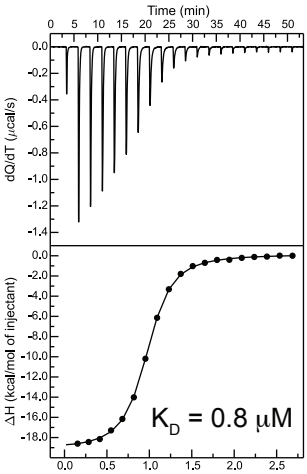

[BRCA2$^{1113\text{-}1129}$ *pS1123*]/ [B56α]

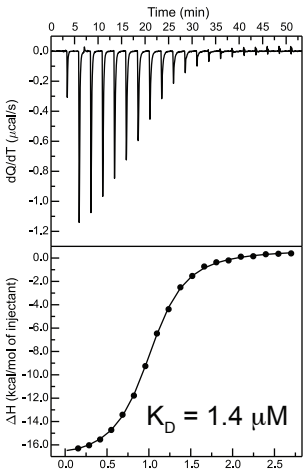

[BRCA2$^{1113\text{-}1129}$ *pT1128*]/ [B56α]

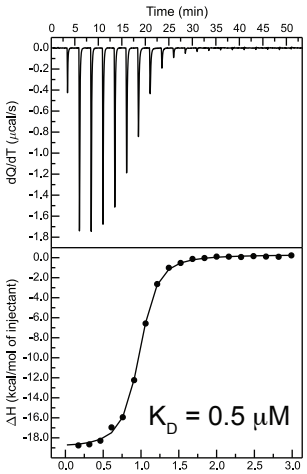

[BRCA2$^{1113\text{-}1129}$ *pS1123, pT1128*]/ [B56α]

Figure S5

Figure S5. Data related to Figure 3.

Isothermal titration calorimetry binding curves for the interaction between the indicated BRCA2 peptides and B56α.

A

B56α complex	K_D (μM)
$BRCA2^{1105-1129}$	7.76 ± 0.40
$BRCA2^{1105-1129}$ S1106R	2.93 ± 0.09
$BRCA2^{1105-1129}$ T1116P	6.92 ± 0.47
$BRCA2^{1105-1129}$ T1128I	7.43 ± 0.43

C

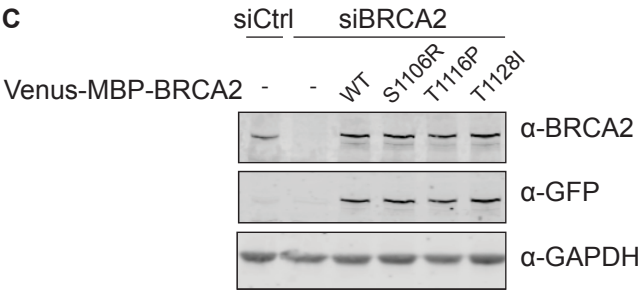

B

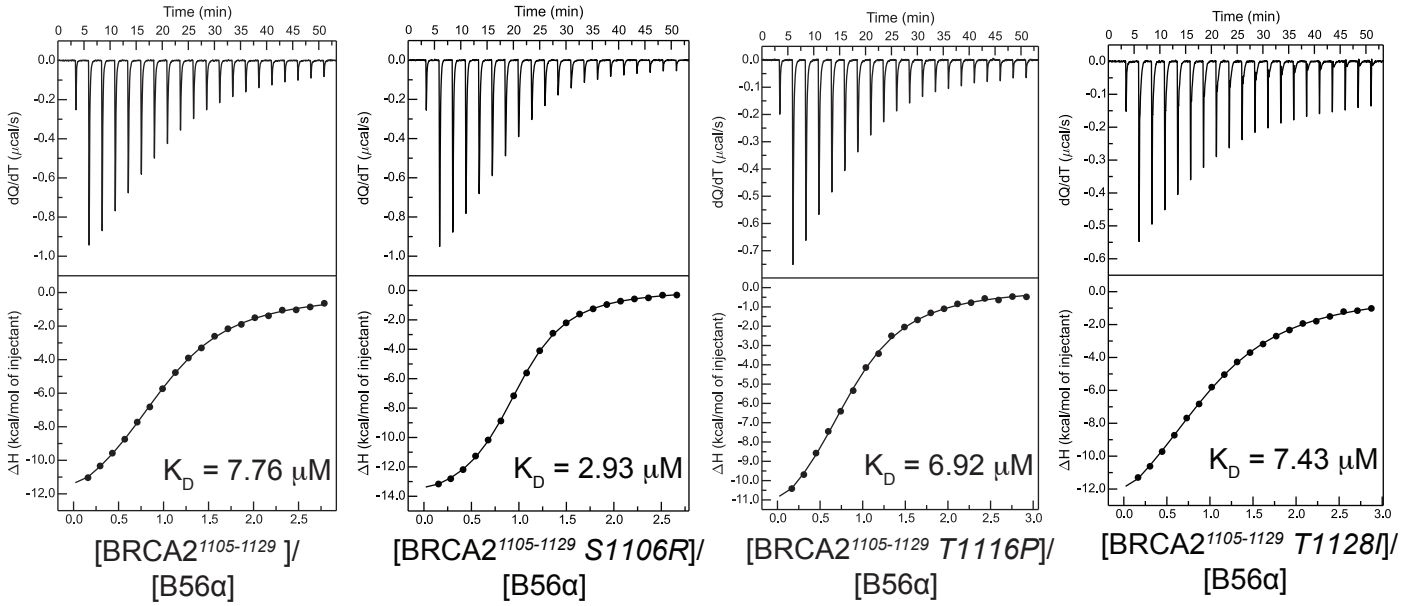

Figure S6.

Figure S6. Data related to Figure 4.

A-B. Dissociation constants (K_D) (A) and binding curves (B) for the interactions between the indicated BRCA2 peptides and B56α measured by isothermal titration calorimetry. The data for BRCA2$^{1105\text{-}1129}$ WT is identical to Fig. 3D and S5. C. Western blot of cell extracts from U2OS Flp-In T-REx cells stably expressing siRNA resistant WT, S1106R, T1116P, and T1128I Venus-MBP-BRCA2 cDNAs, which were transfected with Ctrl or BRCA2 siRNA.

Table S1. Conservation of the BRCA2 B56 binding motif (available as separate file).

Clustal Omega sequence alignment of 190 vertebrate BRCA2 protein sequences. The region around the B56 binding motif is shown. Related to Figure 1.

Table S2. Mass spectrometry data (available as separate file).

Mass spectrometry data of Venus-BRCA2$^{1001\text{-}1255}$ and Venus specific interactors in HeLa cells. Additionally, mass spectrometry data of biotinylated proteins from HeLa Flp-In T-REx TurboID-B56γ cells. Related to Figure 1.

Table S3. Isothermal titration calorimetry data (available as separate file).

Affinities and thermodynamic values of B56α, BRCA2 peptide binding events inferred from ITC measurements performed at 25°C. Gibbs free energy (ΔG), enthalpy (ΔH), entropy (-TΔS), equilibrium dissociation constant (K_D) and reaction stoichiometry (n) are shown. The affinity is defined by the Gibbs energy for binding $\Delta G = -RT \ln K_A = RT \ln K_D$. Related to Figure 1, 3, and 4.

870 **Table S4. DNA oligos.**

871 DNA oligos used in this study. QC: Quick change, F: Forward, R: Reverse.

Primer	Sequence (5'-3')
QC R for resistance to s2084 and s2085	GGAGAAGACATCATCTGGCCTGTATATCTTTCGCAATGAAAGAG
QC F for resistance to s2084 and s2085	CTCTTTCATTGCGAAAGATATACAGGCCAGATGATGTCTTCTCC
QC R to introduce L1114A-I1117A	CCTGATTCTTCTAATGCAGTAGAAGCTTCTGTAATTTCTGC
QC F to introduce L1114A-I1117A	GCAGAAATTACAGAAGCTTCTACTGCATTAGAAGAATCAGG
QC R to introduce S1106A	CTGCCTTTTGGGCAGGTGTTAAATTATGG
QC F to introduce S1106A	CCATAATTTAACACCTGCCCAAAAGGCAG
QC R to introduce S1123A	GCAAATTCAAACTGAGCTCCTGATTCTTC
QC F to introduce S1123A	GAAGAATCAGGAGCTCAGTTTGAATTTGC
QC R to introduce T1128A	GCTTTCTAAACTGAGCAAATTCAAACTG
QC F to introduce T1128A	CAGTTTGAATTTGCTCAGTTTAGAAAGC
F BRCA2 (to introduce Δ1100-113, 2 step)	CCCGGGGGTACCCCACCATGCCTATTGGATCCAAAGAGAGG
R BRCA2 1099 (to introduce Δ1100-1131, 2 step)	TATGTAGCTTGGCTTTGAATTAAAATCCTGCTTGG
F BRCA2 1132 (to introduce Δ1100-113, 2 step)	CAGGATTTTAATTCAAAGCCAAGCTACATATTGC
R BRCA2 (to introduce Δ1100-113, 2 step)	CCCGGGGCGGCCGCCCGATATATTTTTTAGTTGTAATTGTGTCC
QC R to introduce S1106D	CTGCCTTTTGGTCAGGTGTTAAATTATGG
QC F to introduce S1106D	CCATAATTTAACACCTGACCAAAAGGCAG
QC R to introduce S1123D	GAGTAAATTCAAACTGATCTCCTGATTCTTC
QC F to introduce S1123D	GAAGAATCAGGAGATCAGTTTGAATTTACTC
QC R to introduce T1128D	GCTTTCTAAACTGATCAAATTCAAACTG
QC F to introduce T1128D	CAGTTTGAATTTGATCAGTTTAGAAAGC
QC R to introduce S1106R	CAAACCATAATTTAACACCTAGGCAAAAGGCAGAAATTACAGAAC
QC F to introduce S1106R	GTTCTGTAATTTCTGCCTTTTGCCTAGGTGTTAAATTATGGTTTG
QC R to introduce T1116P	AGGCAGAAATTACAGAACTTTCTCCTATATTAGAAGAATCAGGAAGT
QC F to introduce T1116P	ACTTCCTGATTCTTCTAATATAGGAGAAAGTTCTGTAATTTCTGCCT
QC R to introduce T1128I	AGAATCAGGAAGTCAGTTTGAATTTATTCAGTTTAGAAAGCCAAGC
QC F to introduce T1128I	GCTTGGCTTTCTAAACTGAATAAATTCAAACTGACTTCCTGATTCT
R to create BamHI-Myc-BRCA2$^{1001-1255}$-NotI	CCCGGGGCGGCCGCTCATACCTCTGCAGAAGTTTCC
F to create BamHI-Myc-BRCA2$^{1001-1255}$-NotI	CCCGGGGGATCCCCACCATGGAACAAAAGTTGATCAGCGA GGAGGACCTGTCAAATCACAGTT TTGGAGG
R to create BamHI-BRCA2$^{1001-1255}$-NotI	CGATGCGGCCGCTTATTCCTCACTAATATTCTC
F to create BamHI-BRCA2$^{1001-1255}$-NotI	CGATGGATCCATCTCCTTGAATATAGAT

872